FINAL REPORT

Intrinsic Scalar Magnetic Gradiometer for Accurate Localization of Magnetic Anomalies

SERDP Project MR19-1379

FEBRUARY 2020

Dr. Rui Zhang
Geometrics, Inc.

SERDP
DOD ▪ EPA ▪ DOE

REPORT DOCUMENTATION PAGE

Form Approved
OMB No. 0704-0188

1. REPORT DATE *(DD-MM-YYYY)*	**2. REPORT TYPE**	**3. DATES COVERED** *(From - To)*
24-02-2020	SERDP Final Report	3/11/2019 - 3/10/2020

4. TITLE AND SUBTITLE

Intrinsic Scalar Magnetic Gradiometer for Accurate Localization of Magnetic Anomalies

5a. CONTRACT NUMBER
19-P-0024

5b. GRANT NUMBER

5c. PROGRAM ELEMENT NUMBER

6. AUTHOR(S)
Dr. Rui Zhang
Geometrics, Inc.

5d. PROJECT NUMBER
MR19-1379

5e. TASK NUMBER

5f. WORK UNIT NUMBER

7. PERFORMING ORGANIZATION NAME(S) AND ADDRESS(ES)
Geometrics, Inc.
2190 Fortune Drive
San Jose, CA, 95131

8. PERFORMING ORGANIZATION REPORT NUMBER
MR19-1379

9. SPONSORING/MONITORING AGENCY NAME(S) AND ADDRESS(ES)
Strategic Environmental Research and Development Program (SERDP)
4800 Mark Center Drive, Suite 17D03
Alexandria, VA 22350-3605

10. SPONSOR/MONITOR'S ACRONYM(S)
SERDP

11. SPONSOR/MONITOR'S REPORT NUMBER(S)
MR19-1379

12. DISTRIBUTION/AVAILABILITY STATEMENT

DISTRIBUTION STATEMENT A. Approved for public release: distribution unlimited.

13. SUPPLEMENTARY NOTES

14. ABSTRACT

Underwater detection and remediation of Unexploded Ordnance (UXO) remains challenging problem for many reasons including the dynamical nature of the environment, limited visibility, mobility of Targets of Interest (ToIs), and the absence of GPS positioning. Even after ToIs have been identified through Wide Area Assessment techniques, the targets have to be accurately reacquired for precise positioning the instrumentation to classify the ToI. The objective of this project is to investigate the feasibility of a magnetic-gradient-based detailed survey technique for real-time ToI localization and potentially for UXO classification enhancement. The localization method requires the development of ultra-sensitive short-baseline scalar magnetic gradiometer with the combined sensitivity and baseline requirements far beyond the capability of any gradiometer composed of individual magnetometers. A proof-of-concept gradiometer is constructed to explore the possibility of meeting the sensitivity and base-line requirements and accuracy of the localization method is studied theoretically based on sensor performance.

15. SUBJECT TERMS

Unexploded Ordnance, UXO, GPS, Targets of Interest, Underwater detection, magnetic gradiometer

16. SECURITY CLASSIFICATION OF:			**17. LIMITATION OF ABSTRACT**	**18. NUMBER OF PAGES**	**19a. NAME OF RESPONSIBLE PERSON**
a. REPORT	**b. ABSTRACT**	**c. THIS PAGE**			Rui Zhang
UNCLASS	UNCLASS	UNCLASS	UNCLASS	38	**19b. TELEPHONE NUMBER** *(Include area code)*
					408-428-4293

Contents

List of Figures

List of Acronyms

cc – cubic centimeter
Cs – cesium
DBR – Distributed Bragg Reflector
DC – Direct Current
DPLL – Digital Phase Locked Loop
DSP – Digital Signal Processing
EM – Electromagnetic
ESTCP – Environmental Security Technology Certification Program
FPGA − Field-programmable Gate Array
FWHM – Full Width at Half Maximum
GPS – Global Positioning System
Hz – Hertz
IC – Integrated Circuit
kHz – kilohertz
MFAM – MicroFabricated Atomic Magnetometer
MHz – megahertz
ms – milli-second
nm – nanometer
nT – nanoTesla
pT – picoTesla
μs – micro-second
μT – microTesla
PLL – Phase Locked Loop
PCB – Printed Circuit Board
rms – Root Mean Square
SERDP – Strategic Environmental Research and Development Program
TDEM – Time-Domain Electromagnetic
ToI – Target of Interest
UXO – Unexploded Ordnance
VCSEL – Vertical Cavity Surface Emitting Laser
3-D – Three-dimensional

List of Keywords

Intrinsic gradiometer, Scalar magnetometer, UXO

Abstract

Introduction and Objectives: Underwater detection and remediation of Unexploded Ordnance (UXO) remains challenging problem for many reasons including the dynamical nature of the environment, limited visibility, mobility of Targets of Interest (ToIs), and the absence of GPS positioning. Even after ToIs have been identified through Wide Area Assessment techniques, the targets have to be accurately reacquired for precise positioning the instrumentation to classify the ToI. The objective of this project is to investigate the feasibility of a magnetic-gradient-based detailed survey technique for real-time ToI localization and potentially for UXO classification enhancement. The localization method requires the development of ultra-sensitive short-baseline scalar magnetic gradiometer with the combined sensitivity and baseline requirements far beyond the capability of any gradiometer composed of individual magnetometers. A proof-of-concept gradiometer is constructed to explore the possibility of meeting the sensitivity and base-line requirements and accuracy of the localization method is studied theoretically based on sensor performance.

Technical Approach: The gradient from a magnetic dipole moment, which is a good model for UXOs, decays as a function of R^{-4}, where R is the distance between the dipole moment and the sensor. If gradients at four different points are measured, the location of the dipole moment can be calculated in the coordinate system defined by the four points. This simple calculation can provide us with a good initial estimate of the dipole location, which can greatly facilitate the full inversion method for achieving better and more complete dipole parameters. The method poses a combined requirement of low noise and short baseline on the gradient measurement, which cannot be met with commercially available magnetometers. We investigate a new intrinsic scalar magnetic gradiometer sensor to address this requirement. The intrinsic gradiometer uses a single far detuned laser beam to probe two atomic ensembles. The intrinsic gradient measurement has the advantage of cancelling out many common-mode noises and hence achieves much better sensitivity.

Results: A magnetic-gradient-based inversion algorithm is developed for real-time localization of a magnetic dipole moment. Our theoretical simulation indicates that accurate real-time localization is possible if the peak-to-peak gradient noise is about 4 pT at 5 cm baseline. For a 100 Hz sample rate, 4 pT peak-to-peak noise is equivalent to about 150 fT/√Hz noise density, which is demonstrated in a magnetically unshielded environment by a prototype portable intrinsic gradiometer constructed using vertical-cavity surface-emitting lasers (VCSELs). Inside a magnetically shielded environment, better than 90 fT/√Hz sensitivity is achieved.

***Benefit*:** This research work eliminates the fundamental scientific risk of obtaining ultra-sensitive short-baseline magnetic gradient data in practical applications. The gradient measurement can be used for real-time UXO localization, greatly reducing the cost of UXO disposal by shortening the time-consuming localization procedure. Current classification methods using time domain electromagnetic (TDEM) require very high accuracy in real-time target localization to position the instrument over the target -- this method enhances reacquisition efficiency and accuracy and may be integrated with TDEM instruments to reduce location-based uncertainty in classification results.

Executive Summary

1. Introduction

Underwater detection and remediation of Unexploded Ordnance (UXO) remains challenging problem for many reasons including the dynamical nature of the environment, limited visibility, mobility of Targets of Interest (ToIs), and the absence of GPS positioning. Even after ToIs have been identified through Wide Area Assessment techniques, the targets have to be accurately reacquired for precise positioning the instrumentation to classify the ToI. Therefore, underwater UXO disposal is a very costly operation. One way to address this issue is to develop more efficient and effective UXO localization techniques.

2. Objectives

The objective of this project is to investigate the feasibility of a magnetic-gradient-based detailed survey technique for real-time ToI localization and potentially for UXO classification enhancement. The localization method requires the development of ultra-sensitive short-baseline scalar magnetic gradiometer with the combined sensitivity and baseline requirements far beyond the capability of any gradiometer composed of individual magnetometers. A proof-of-concept gradiometer is constructed to explore the possibility of meeting the sensitivity and base-line requirements and accuracy of the localization method is studied theoretically based on sensor performance.

3. Technical Approach

The magnetic field generated by the UXOs can be well represented by a magnetic dipole moment. Based on the properties of a dipole field, the gradient is proportional to R^{-4}, where R is the distance from the dipole to the point of interest. Assume that we measure the total field gradient, defined as $\Delta B = \sqrt{[(dB/dx)^2+[(dB/dy)^2+[(dB/dz)^2]}$, at four locations indicated by the red dots shown in Figure 1. A Cartesian coordinate system is defined by the four points with point 0 being the origin. The other 3 points are located at (x_1, 0, 0), (0, y_2, 0) and (0, 0, z_3) in this system. If a magnetic dipole is located at (x, y, z), the measured field gradient should satisfy the following equations:

$$\Delta B_i = M_i R_i^{-4}, \qquad i = 0, 1, 2, 3$$

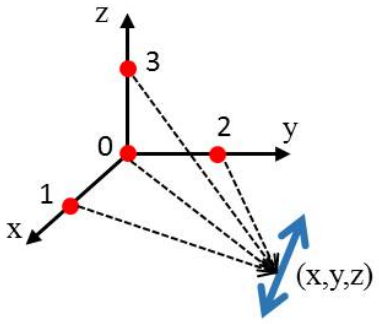

Figure 1 Schematic showing the relative position between a dipole moment and four points of interest. The position of the dipole moment, in the Cartesian coordinate defined by the four observation points, can be calculated based on the four total gradients.

In principle, the parameter M_i slightly depends on the direction of R_i and the orientation of the dipole moment. However, in most cases, M_i does not change too much if the solid angle defined by the four points with respect to the center of the dipole is not large. Therefore, we can assume that M_i only depends on the magnitude of the magnetic dipole and is the same at four locations. Under this assumption, we have four equations with four variables (x, y, z) and M. We can now solve the equations for the location of the dipole moment, (x, y, z). The analytically obtained solution (x, y, z, M) is then set as the starting point for the following gradient-based inversion method which calculates the dipole parameters numerically.

The magnetic field of a dipole is given by $\boldsymbol{B}_{dipole} = \frac{\mu_0}{4\pi}\left[\frac{3\hat{r}(\boldsymbol{m}\cdot\hat{r})-\boldsymbol{m}}{r^3}\right]$, where μ_0 is the vacuum permeability, $\boldsymbol{m}$ is the vector dipole moment, $\hat{r}$ is the unit vector in the direction of $\boldsymbol{r}$ which is the relative location of the point of interest with respect to the magnetic dipole. With a known background magnetic field $\boldsymbol{B}_0$, the magnetic field of the dipole can be calculated at any location $\boldsymbol{r}$. Based on this, we first establish a full dipole field model, which outputs $\boldsymbol{B}(\boldsymbol{m}, \boldsymbol{B}_0, \boldsymbol{r})$ with input parameters ($\boldsymbol{m}$, $\boldsymbol{B}_0$, $\boldsymbol{r}$). With the function $\boldsymbol{B}(\boldsymbol{m}, \boldsymbol{B}_0, \boldsymbol{r})$, it is straightforward to calculate magnetic gradients. The relative location $\boldsymbol{r}$ can be expressed as $\boldsymbol{r} = \boldsymbol{r}_i - \boldsymbol{r}_d$, where $\boldsymbol{r}_i$ is the observing point location and $\boldsymbol{r}_d$ is the dipole location. Now the total gradients at four observing points, shown in Figure 1, can be expressed as $\Delta B_i(\boldsymbol{m}, \boldsymbol{r}_d, \boldsymbol{B}_0, \boldsymbol{r}_i)$, i = 1, 2, 3, 4. To improve the localization accuracy, we also include four vertical gradients in the simulation, $\Delta B_{zi}(\boldsymbol{m}, \boldsymbol{r}_d, \boldsymbol{B}_0, \boldsymbol{r}_i)$, i = 1, 2, 3, 4. All simulation codes are written in Matlab.

The gradient-based localization method can now be simplified as how to find ($\boldsymbol{m}$, $\boldsymbol{r}_d$) with a given set of data, (ΔB_i, ΔB_{zi}, $\boldsymbol{B}_0$, $\boldsymbol{r}_i$). There are no analytical expressions for ($\boldsymbol{m}$, $\boldsymbol{r}_d$) in terms of (ΔB_i, ΔB_{zi}, $\boldsymbol{B}_0$, $\boldsymbol{r}_i$). Therefore, we construct the following function:

$$F(\boldsymbol{m}, \boldsymbol{r_d}) = \sum_{i=1}^{4}\left[\frac{\Delta B_i(\boldsymbol{m}, \boldsymbol{r_d}, \boldsymbol{B_0}, \boldsymbol{r_i})}{\Delta B_i^0} - 1\right]^2 + \sum_{i=1}^{4}\left[\frac{\Delta B_{zi}(\boldsymbol{m}, \boldsymbol{r_d}, \boldsymbol{B_0}, \boldsymbol{r_i})}{\Delta B_{zi}^0} - 1\right]^2$$

Here ΔB_i^0 and ΔB_{zi}^0 are measured magnetic gradients at the four points of interest. The best set of dipole parameters ($\boldsymbol{m}$, $\boldsymbol{r}_d$) should minimize the function $F(\boldsymbol{m}, \boldsymbol{r}_d)$. To avoid the function being dominated by measured gradients with close to zero values, additional weight parameters are included:

$$G(\boldsymbol{m}, \boldsymbol{r_d}) = \sum_{i=1}^{4}\left|\frac{\Delta B_i^0}{\max(\Delta B_i^0)}\right| * \left[\frac{\Delta B_i(\boldsymbol{m}, \boldsymbol{r_d}, \boldsymbol{B_0}, \boldsymbol{r_i})}{\Delta B_i^0} - 1\right]^2 + \sum_{i=1}^{4}\left|\frac{\Delta B_{zi}^0}{\max(\Delta B_i^0)}\right| * \left[\frac{\Delta B_{zi}(\boldsymbol{m}, \boldsymbol{r_d}, \boldsymbol{B_0}, \boldsymbol{r_i})}{\Delta B_{zi}^0} - 1\right]^2$$

With a given set of parameters (ΔB_i^0, ΔB_{zi}^0, $\boldsymbol{B}_0$, $\boldsymbol{r}_i$), we find the minimum value of $G(\boldsymbol{m}, \boldsymbol{r}_d)$ with the built-in Matlab function, *fminsearch*. The corresponding solution ($\boldsymbol{m}$, $\boldsymbol{r}_d$) provides us with information about the magnetic dipole, including its location, $\boldsymbol{r}_d$. The starting dipole magnitude and location is given by the analytical solution and the initial dipole orientation is defined by the background magnetic field direction.

The gradient-based localization method imposes significantly stringent requirements on the performance of the magnetometer. A much better sensitivity is needed since the gradient signal will be much smaller. This is because not only the gradient signal decays much faster as a function

of distance, but also a small baseline measurement is necessary. The smaller the baseline, the closer the measurement is to the true gradient and less affected by the background noise. In addition, due to the small baseline requirement, the magnetometer needs to be small in size and free from measurement interference. At present, such magnetometers are not commercially available. Even in research labs, scalar magnetometers with sub-pT/√Hz sensitivity using miniaturized cells and vertical-cavity surface-emitting lasers (VCSELs), two components essential for achieving a small sensor package, have not been demonstrated.

Over the past several years with support from SERDP under projects MM-1512, MM1568 and MR-2104, Geometrics has put in significant amount of effort in developing and successfully commercialized a high performance, small size, all-optical scalar magnetometer called the MFAM. A sensitivity of 1 pT/√Hz is routinely achieved in commercially available sensors of volume less than 20 cc. Our research reveals that the sensitivity of the MFAM is mainly limited by the probe VCSEL since it is tuned to be resonant with an atomic transition. The resonant probe light interacts strongly with the atoms, not only depolarizing the synchronized atomic spin, but also introducing more noise into the signal by converting laser frequency noise into the laser intensity noise, which limits the signal-to-noise ratio (SNR) of the measurement. With commercially available narrow-linewidth distributed Bragg reflection (DBR) lasers and off-resonant detection of the atomic precession, we have demonstrated more than an order of magnitude improvement in sensitivity in the same cell as used in the MFAM magnetometer.

There are two main factors affecting the sensitivity of sensors using VCSEL lasers, frequency stabilization and laser linewidth. Both the operating current and the temperature of the laser affect its frequency. The most common frequency stabilization method is to locks the laser to the resonant frequency of an atomic transition using laser current servo. The method, however, cannot be used for off-resonant frequency, which is necessary for better sensor performances. Here we will explore the possibility of off-resonant frequency stabilization by temperature servo of the VCSEL die at a fixed operating current. The other factor, laser linewidth, characterizes the fundamental limit on the laser frequency uncertainty. Commercial DBR lasers normally have linewidths ranging from sub-MHz to several MHz. On the other hand, VCSELs have much wider linewidths, typically around 100 MHz. The large noise in the probe laser frequency increases the noise in the detected precession signal, hence affecting the magnetometer sensitivity. Here we propose an intrinsic gradiometer setup, which minimizes the impact of the laser frequency noise on the gradiometer sensitivity.

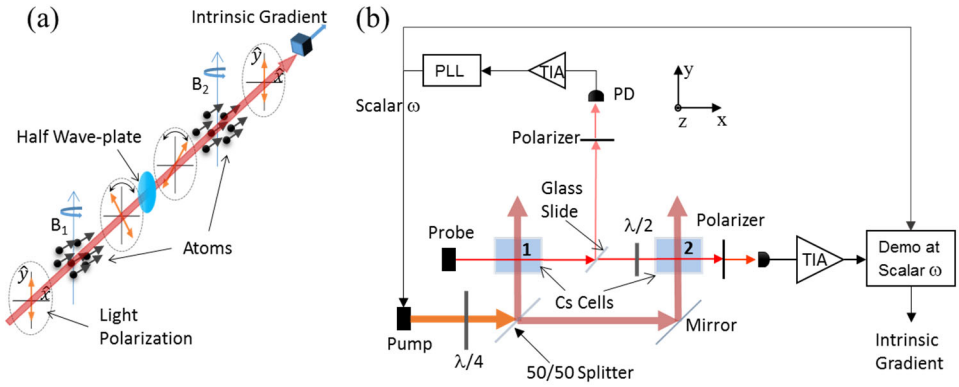

Figure 2 (a) Basic operating principle of an intrinsic gradiometer. (b) Schematics of the intrinsic gradiometer.

The basic principle behind the intrinsic gradiometer is illustrated in Figure 2 (a). A single linearly-polarized off-resonant probe interrogates two atomic ensembles separated by a baseline distance. The atoms at both locations are spin-polarized exactly the same way. After interacting with the first atomic ensemble, the probe goes through a half-wave plate oriented such that the acquired polarization rotation of the probe beam is reversed, as shown in the figure. If the magnetic fields at the two locations are exactly the same, the second ensemble of atoms rotates the probe polarization back to its original position. The optical rotation effect is cancelled. However, if there is a magnetic field gradient, the difference in precession frequencies will result in non-cancellation in the rotation of the probe polarization. Therefore, the probe polarization signal is a direct measurement of the magnetic field gradient.

The intrinsic gradiometer can be realized schematically shown in Figure 2 (b). A circularly polarized pump beam is equally split into two beams, exciting Cs atoms at two vapor cells. A linearly polarized off-resonant probe beam interrogates two atomic ensembles at the same time. About 10% light is split from the main probe beam by a piece of glass slide and is detected by a photodiode after an analyzing linear polarizer. The photodiode current is then amplified and sent to a phase-lock-loop (PLL) circuit. The output of the PLL drives the pump laser through current modulation and is the scalar measurement of the magnetic field at the first cell. After the second cell, the main probe beam is analyzed by a linear polarizer and detected by a photodiode, whose current is amplified and sent to a demodulator with its reference frequency determined by the PLL output. The quadrature component of the demodulated probe signal is converted to the intrinsic gradiometer reading with a constant determined by the slope of the quadrature component at the magnetic resonance.

4. Results and Discussion

The "measured" gradients (ΔB_i^0, ΔB_{zi}^0) are generated by a theoretical model described in the Materials and Methods section and in reference [1]. A noise source is also created by multiplying a random number between -1 and 1 with a fixed value and added to each gradient in (ΔB_i^0, ΔB_{zi}^0) to represent the measurement error caused by sensor output noise. The fixed value is the peak-to-peak noise amplitude. We apply the inversion method to the gradient data sets generated by a 10cm (diameter) x 30 cm (length) spheroid with its orientation and location given in the first two rows of Table 1. The background magnetic field has a magnitude of 50 μT and in (30°, 0) direction. The peak-to-peak sensor noise is first set at 4 pT. The inversion simulation is then run 10 times for each set of gradient data to account for the random noise. The inversion time is typically less than half a second for each run. The resulting averaged dipole locations and standard deviations are shown in Table 1 third row. As seen, the computed dipole locations from the inversion simulations are almost identical to the set dipole locations for the first 5 cases. The accuracy of the inversion method decreases for the last 3 cases due to lower gradient signal levels. Nevertheless, the errors are still within 5 cm. We also increase the peak-to-peak sensor noise to 40 pT. The corresponding inversion results are shown in Table 1 fourth row. The inversion accuracy becomes much worse and the method fails for the last case. This is not surprising since the gradient signals are only about 100 pT, comparable to the noise level.

Table 1 Localization results from the inversion method for different magnetic dipoles. The dipole gradients are generated by a spheroid with its orientation and location given in the first two rows.

Orientation (θ, φ)	0°,0°	30°,0°	60°,0°	90°,0°	120°,0°	0°,0°	30°,60°	60°,90°
Set Location (x, y, z)	1 m, 1 m, -1 m	1 m, 1 m, -1 m	1 m, 1 m, -1 m	1 m, 1 m, -1 m	1 m, 1 m, -1 m	1 m, 2 m, -1 m	2 m, 1 m, -0.5 m	2 m, 1 m, -0.5 m
Inversion Results $4pT_{p-p}$ noise	1 ±0.009 m, 1 ±0.007 m, -1 ±0.008 m	1 ±0.001 m, 1 ±0.005 m, -1 ±0.007 m	1 ±0.007 m, 1 ±0.007 m, -1 ±0.01 m	1 ±0.001 m, 1.01±0.006 m, -1 ±0.02 m	0.99±0.01 m, 1 ±0.01 m, -1 ±0.02 m	0.98±0.04 m, 2 ±0.03 m, -1.04 ±0.06 m	1.99 ±0.04 m, 1.01 ±0.02 m, -0.51 ±0.04 m	1.97 ±0.08 m, 1.04 ±0.08 m, -0.49 ±0.08 m
Inversion Results $40pT_{p-p}$ noise	0.99 ±0.09 m, 1.01 ±0.06 m, -0.97 ±0.1 m	1 ±0.04 m, 1.05 ±0.08 m, -0.92 ±0.1 m	0.98 ±0.04 m, 0.98 ±0.07 m, -1.02 ±0.07 m	0.99 ±0.06 m, 1.01 ±0.06 m, -0.97 ±0.1 m	1.1 ±0.2 m, 1.08 ±0.2 m, -0.74 ±0.4 m	1.01 ±0.7 m, 1.78 ±0.7 m, -1.57 ±1 m	1.88 ±0.6 m, 1.11 ±0.4 m, -0.45 ±0.4 m	0.88 ±0.8 m, 0.18 ±0.9 m, -1.76 ±1.6 m

Based on the results shown in Table 1, 4 pT peak-to-peak sensor output noise is required for the gradient-based inversion method. If we assume a 10 ms measurement time, 4 pT peak-to-peak noise is equivalent to a rms noise density of about 100 fT/√Hz, which is an order of magnitude less than the noise density achieved in our MFAM sensors. Much better sensors need to be developed for the gradient based inversion method.

A portable intrinsic gradiometer is constructed to investigate the feasibility of meeting the sensitivity and baseline requirement. The gradiometer consists of two miniaturized Cs vapor cells (cubic, 5mm inner dimension) separated by 5 cm. Two VCSEL lasers output pump and probe beams as shown in Figure 2 (b). The PLL and the demodulator are implemented using a commercial lock-in amplifier from Zurich instrument. The sensitivity of the gradiometer is tested inside a magnetic shield can. The setup is shown in Figure 3.

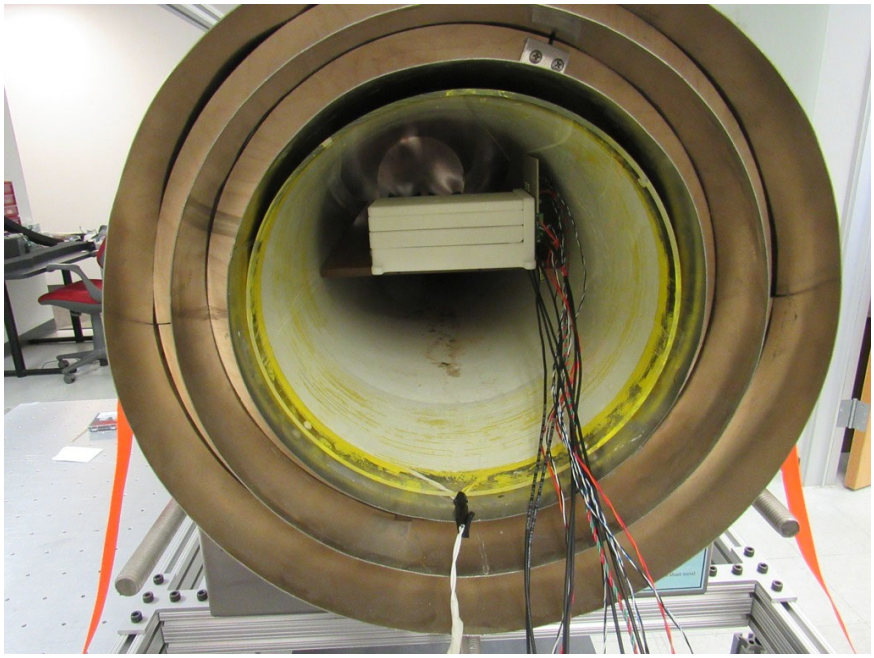

Figure 3 Portable intrinsic gradiometer tested inside a shield can.

To investigate the noise performance of the gradiometer, a magnetic field is generated inside the shield can using a solenoid controlled by a home-made ultra-low-noise current source. The field strength is set to be about 63,600 nT. We record both the scalar and the gradiometer outputs for 5 minutes and plot their noise densities in Figure 4. As seen, the gradiometer sensitivity can reach below 90 fT/√Hz, which meets the sensitivity requirement of the gradient-based inversion method. The sharp spikes are due to the couplings of the 60 Hz power line radiation and its harmonics into the electronics.

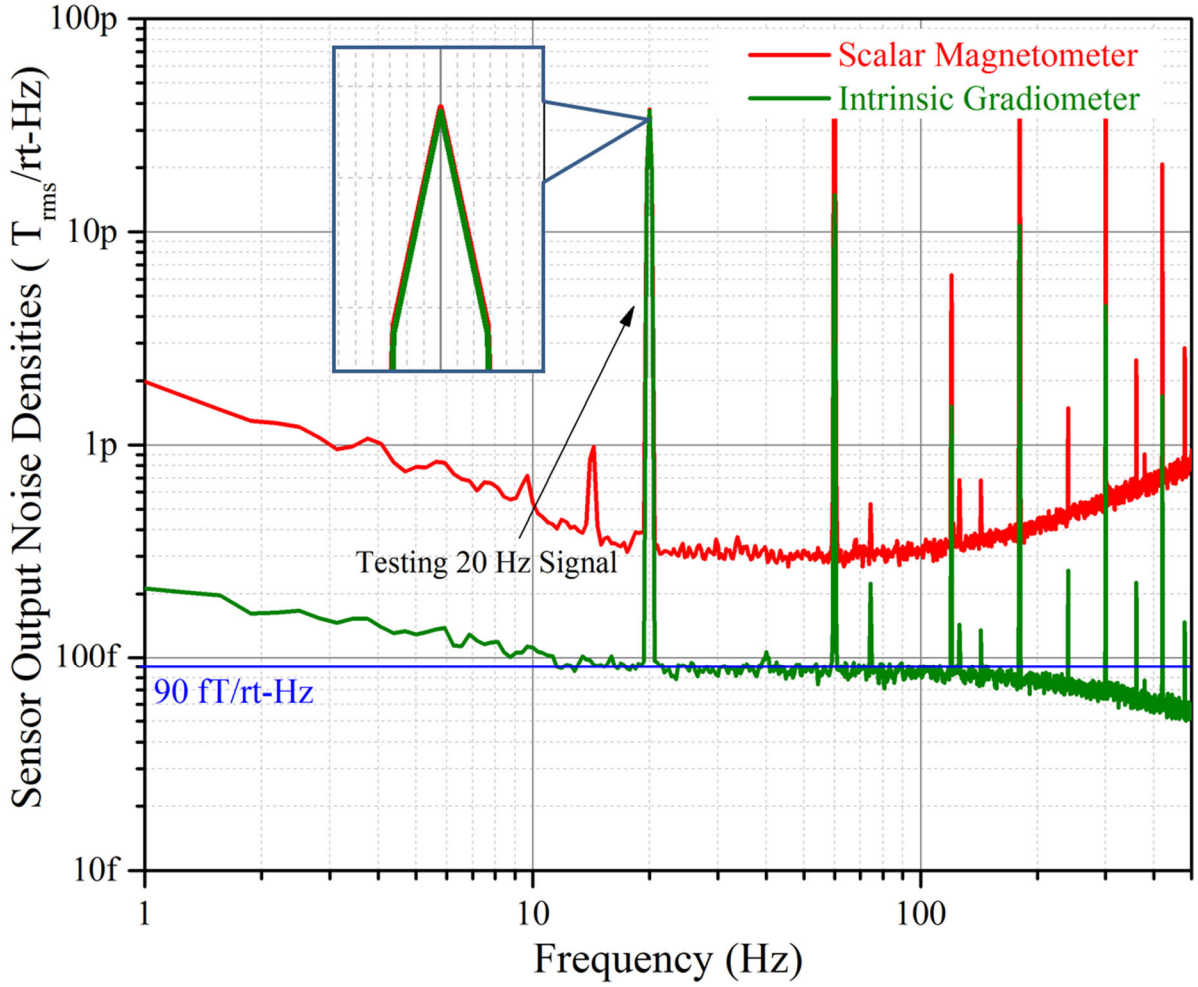

Figure 4 Output noise densities of both the scalar magnetometer (red curve) and the intrinsic gradiometer (green curve). A 20 Hz testing signal is also generated by a 3 mm diameter coil right next to the first cell. The signal should have the same amplitude in both outputs.

As shown in Figure 2 (b), the gradiometer is operated in open-loop mode, whose output is converted from the quadrature component of the demodulated probe signal with a constant determined by the magnetic resonance.We need to verify the accuracy of the conversion constant. This is done using a 20 Hz testing signal. The signal is generated by a 3 mm diameter coil attached to the first cell. Due to the coil size and the distance between the coil and the second cell (> 5cm), the signal at the second cell should be 3 orders of magnitude smaller than that at the first cell. Therefore the amplitude of the 20 Hz testing signal measured by the scalar magnetometer (measuring fields at the first cell) should be the same as that measured by the intrinsic gradiometer if the gradient conversion coefficient is accurate. As seen in Figure 4, the 20 Hz signal measured

by the intrinsic gradiometer (green curve) has the same amplitude as that of the scalar magnetometer (red curve). This confirms the accuracy of the conversion coefficient.

5. Implications for Future Research and Benefits

A portable intrinsic gradiometer is shown to meet the sensitivity and baseline requirements of a magnetic-gradient-based inversion algorithm for real-time localization of a magnetic dipole moment. A gradient measurement with better than 100 fT/√Hz sensitivity at 5 cm baseline is achieved. The successfully demonstrated portable gradiometer is composed of miniaturized vapor cells and VCSEL lasers, two components essential for achieving compact sensor packages. The success of the project eliminates the fundamental scientific risk of obtaining ultra-sensitive short-baseline magnetic gradient data in practical applications.

The gradient measurement can be used for real-time UXO localization with high accuracy, greatly reducing the cost of UXO disposal by shortening the time-consuming localization procedure. Current classification methods using time domain electromagnetic (TDEM) require very high accuracy in real-time target localization to position the instrument over the target – this new localization method enhances reacquisition efficiency and accuracy and may be integrated with TDEM instruments to reduce location-based uncertainty in classification results.

More efforts are necessary towards a field demonstration of the gradient-based real-time UXO localization. The next step is to design a more-compact sensor package and develop an integrated sensor driver. More theoretical modeling work is also needed to study the impact of multiple UXOs on the localization accuracy. These efforts can lead to magnetic gradient measurement with unprecedented sensitivities and short-baselines and hence may enable many more novel applications of the magnetic gradiometry in UXO detection and classification.

Objective

The objective of this project is to investigate the feasibility of a magnetic-gradient-based detailed survey technique for real-time Target of Interest (ToI) localization and potentially for Unexploded Ordnance (UXO) classification enhancement. The localization method requires the development of ultra-sensitive short-baseline scalar magnetic gradiometer with the combined sensitivity and baseline requirements far beyond the capability of any gradiometer composed of individual magnetometers. A proof-of-concept gradiometer is constructed to explore the possibility of meeting the sensitivity and base-line requirements and accuracy of the localization method is studied theoretically based on sensor performance. This project relates to MRSEED-19-S1, Detection, Classification, and Remediation of Military Munitions Underwater. We investigate new analysis methodologies to characterize the full parameters of a magnetic dipole moment based on the gradient measurement in the far field, as well as the development of sensors needed to meet the requirements of these techniques. The successful development of these techniques will greatly improve the efficiency of localizing UXOs, particularly in a dynamic underwater environment with high UXO mobility and limited access to location information.

Background

Underwater detection and remediation of Unexploded Ordnance (UXO) remains challenging problem for many reasons including the dynamical nature of the environment, limited visibility, mobility of Targets of Interest (ToIs), and the absence of GPS positioning. Even after ToIs have been identified through Wide Area Assessment techniques, the targets have to be accurately reacquired for precise positioning the instrumentation to classify the ToI. In this research work, we investigate the feasibility of a magnetic-gradient-based detailed survey technique for real-time ToI localization and potentially for UXO classification enhancement. Gradiometer system consisted of multiple scalar magnetometers has been studied for UXO [2, 3] since it is well known that the gradient measurement can obtain more information than the scalar field measurement. However, commercially available magnetometers are either not very sensitive, like fluxgates, or too bulky and often not free from RF interference, such as traditional Cesium magnetometers. Ultra-sensitive small-baseline gradient measurement has NOT been available outside advanced research labs. Recently Geometrics successfully commercialized the MFAM technology, a miniaturized all-optical Cesium magnetometer, the development of which is partly supported by SERDP through project MM-1512, MM-1568 and MR-2104. The MFAM sensor has a size of less than 20 cubic centimeters and reaches 1 pT/√Hz sensitivity. Our research also indicates that the MFAM sensitivity is mainly limited by the on-resonant absorption measurement of the atomic precession. More complicated atomic-precession-detection schemes, such as off-resonant optical rotation measurement, can greatly improve the magnetometer sensitivity. However, such a scheme has never been implemented in compact sensors, mainly due to the challenge of stabilizing vertical-cavity surface-emitting lasers (VCSELs) at off-resonant frequencies. In addition, we investigate a novel intrinsic scalar magnetic gradiometer, which directly reads out the magnetic gradient through a single off-resonant laser beam probing two atomic ensembles at the same time. The intrinsic gradiometer can improve the gradient noise by at least a factor of √2, compared with a conventional gradiometer composed of two individual magnetometers. This work can lead to magnetic gradient measurement with unprecedented sensitivities and hence enable many new applications of the magnetic gradiometry, one of which is also explored theoretically in this project for fast UXO localization.

Materials and Methods

1. Gradient-Based Fast Localization of Magnetic Anomalies

The magnetic field generated by the UXOs can be well represented by a magnetic dipole moment. Based on the properties of a dipole field, the gradient is proportional to R^{-4}, where R is the distance from the dipole to the point of interest. Assume that we measure the total field gradient, defined as $\Delta B = \sqrt{[(dB/dx)^2+[(dB/dy)^2+[(dB/dz)^2]}$, at four locations indicated by the red dots shown in Figure 5. A Cartesian coordinate system is defined by the four points with point 0 being the origin. The other 3 points are located at (x_1, 0, 0), (0, y_2, 0) and (0, 0, z_3) in this system. If a magnetic dipole is located at (x, y, z), the measured field gradient should satisfy the following equations:

$$\Delta B_i = M_i R_i^{-4}, \qquad i = 0, 1, 2, 3 \qquad (1)$$

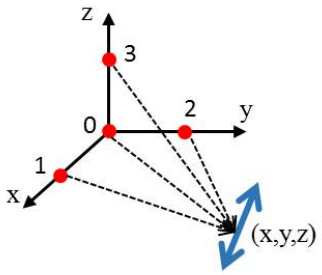

Figure 5 Schematic showing the relative position between a dipole moment and four points of interest. The position of the dipole moment, in the Cartesian coordinate defined by the four observation points, can be calculated based on the four total gradients.

In principle, the parameter M_i slightly depends on the direction of R_i and the orientation of the dipole moment. However, in most cases, M_i does not change too much if the solid angle defined by the four points with respect to the center of the dipole is not large. Therefore, we can assume that M_i only depends on the magnitude of the magnetic dipole and is the same at four locations. Under this assumption, we have four equations with four unknowns (x, y, z) and M. We can now solve the equations for the location of the dipole moment, (x, y, z).

To develop a model describing this method, we first calculate the magnetic field generated by an UXO, approximated as a spheroid, in the Earth's magnetic field. The theoretical model is based on the reference [1]. The spheroid is characterized by eight parameters, (x_0, y_0, z_0, θ, φ, a, e, μ). The location of the spheroid is given by (x_0, y_0, z_0) with ground being at z = 0 and negative z indicating underground. The spheroid has a diameter of a, aspect ratio of e (length = a×e) and permeability of μ.The symmetric axis of the spheroid points in the (θ, φ) direction, with θ being the polar angle and φ being the azimuth. The Earth's magnetic field has a magnitude of 50 μT and in (30°, 0) direction, indicated by three arrows in Figure 6. With the spheroid parameters and the Earth's magnetic field, the induced magnetic dipole moment can be calculated. The dipole approximation is valid as long as the distance between the spheroid and the observation point is greater than a few body lengths of the spheroid. With the induced dipole moment and the Earth's

magnetic field, the magnitude of the combined field can be computed at any location. In the following sections, the diameter *a*, aspect ratio *e* and permeability μ of the spheroid are fixed at 10 cm, 3 and 200, respectively.

We set the location (x_0, y_0, z_0) and the orientation (θ, φ) of the spheroid and compute the total field gradient, ΔB, at four points, (0, 0, 0) (20 cm, 0, 0) (0, 20 cm, 0) and (0, 0, 20 cm) according to the forward model. The gradient baseline is 5 cm. Based on the Equation (1), with four measurements of ΔB at four locations, the (x, y, z) coordinates of the dipole moment can be calculated. We compare the set coordinate (x_0, y_0, z_0) and the calculated coordinate (x, y, z) to determine the validity and accuracy of the proposed UXO localization method.

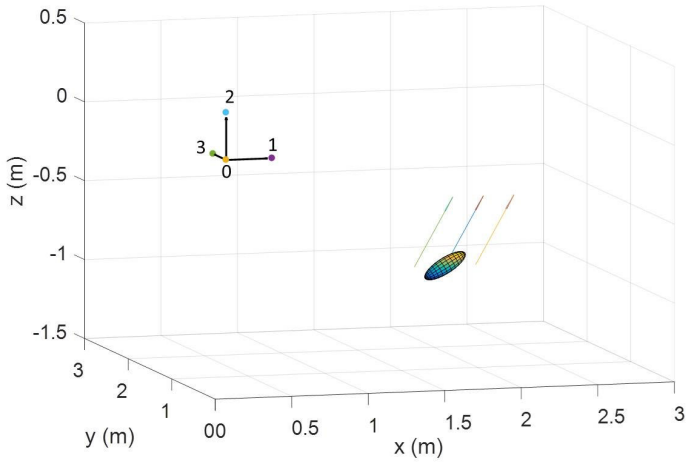

Figure 6 Relative position and orientation of an UXO (modeled by the spheroid) in the earth's magnetic field (indicated by the arrows). The four points where the total magnetic field gradient is measured define the cartesian coordinate. The induced dipole field of the spheroids is calculated in the forward model.

We also try to calculate the (x, y, z) based on the scalar field, B, since the dipole magnetic field is proportional to R^{-3}. The difference between B and the Earth's magnetic field is used as the magnitude of the dipole field. The results show that the scalar-field-based inversion, although being much simpler compared with the gradient-based method, lacks accuracy in determining the location of the dipole moment and in some cases, the results are invalid.

In Table 2, we choose 8 different combinations of orientation and location of the spheroid, shown in the first two rows of the Table. The corresponding calculated spheroid location is shown in row 3 or row 4 based on the total gradient or the total field, respectively. As seen, the gradient-based method produces much more accurate results. The measurement errors are less than 30 cm, mostly within 20 cm, for a spheroid distance of more than 1.5 m. The total field-based method, in some cases (shown as red) however, can lead to errors so large that we cannot consider the measurement valid any more. The inaccuracy of the gradient-based method and the failure of the total field-based method are mainly due to how the dipole field is measured. Since the Earth's magnetic field is always present and much higher in strength than that due to the dipole, only the projection of the dipole field onto the Earth's field can be measured. At locations where the dipole field is close to orthogonal to the Earth's field, it is the direction, not the magnitude, of the dipole field that

determines the measured total field, essentially making the R^{-3} proportionality invalid. The total gradient measurement, on the other hand, is less affected by the projection.

To obtain more accurate measurements, we will need the full dipole field model, including the dipole orientation and the projection onto the Earth's field. In principal, with ΔB measurements at two more locations, the orientation, (θ, φ), of the dipole moment can also be determined since we now have 6 equations for 6 unknowns, (θ, φ, M, x, y, z), assuming that the magnitude and orientation of the Earth's magnetic field are known. However, the analytical expression for ΔB based on (θ, φ, M, x, y, z) is extremely complicated and highly non-linear. Therefore, the inversion from ΔB to estimate (θ, φ, M, x, y, z) need fairly sophisticated and computationally intensive optimization methods, which might preclude real-time implementation. From the discussion above, it is possible to achieve reasonably close solutions of (x, y, z) and maybe M as well. We can then rely on the forward model to determine the orientation, (θ, φ), by finding the results best matching the measured ΔB values. We can further verify the answer by checking the total field measurements.

Table 2 Comparison of the gradient-based and total field-based methods in determining the location of a dipole moment. The spheroid orientation and true location are given in the first two rows.

Orientation (θ, φ)	0°,0°	30°,0°	60°,0°	90°,0°	120°,0°	0°,0°	30°,60°	60°,90°
Set Location (x, y, z)	1 m, 1 m, -1 m	1 m, 1 m, -1 m	1 m, 1 m, -1 m	1 m, 1 m, -1 m	1 m, 1 m, -1 m	1 m, 2 m, -1 m	2 m, 1 m, -0.5 m	2 m, 1 m, -0.5 m
Measured Location Gradient Based	0.98 m, 1.02 m, -1.06 m	0.83 m, 0.92 m, -1.20 m	0.88 m, 0.97 m, -1.10 m	0.87 m, 1.01 m, -1.04 m	0.82 m, 0.95 m, -1.18 m	0.81 m, 1.91 m, -1.27 m	2.02 m, 1.01 m, -0.27 m	2.01 m, 1.01 m, -0.26 m
Measured Location Total Field Based	0.02 m, 0.21 m, -0.69 m	0.21 m, 0.43 m, -1.00 m	0.53 m, 0.73 m, -1.11 m	0.83 m, 0.93 m, -0.94 m	0.20 m, 0.47 m, -1.09 m	0.15 m, 0.76 m, -1.33 m	1.75 m, 0.87 m, 0.46 m	1.41 m, 0.81 m, 0.68 m

2. Intrinsic Scalar Magnetic Gradiometer

As discussed above, the gradient-based UXO localization method can produce much better results than the total field-based one. However, the gradient measurement also imposes significantly stringent requirements on the performance of the magnetometer. For instance, a much better sensitivity is needed since the gradient signal will be much smaller. This is because not only the gradient signal decays much faster as a function of distance, but also a small baseline measurement is necessary. For example, 100 fT/√Hz sensitivity is required for detecting the 30 cm object at a

distance of 5 m. Similarly, the smaller the baseline, the closer the measurement is to the true gradient and less affected by the background noise. In addition, due to the small baseline requirement, the magnetometer needs to be small in size and free from measurement interference. At present, such magnetometers are not commercially available. Even in research labs, scalar magnetometers having sub-pT/√Hz sensitivity using miniaturized cells and using vertical-cavity surface-emitting lasers (VCSELs), two components essential for achieving a small sensor package, have not been demonstrated.

Over the past several years with support from SERDP under projects MM-1512, MM1568 and MR-2104, Geometrics has put in significant amount of effort in developing and successfully commercialized a high performance, small size, all-optical scalar magnetometer called the MFAM. The MFAM uses a pump-probe Bell-Bloom [4] scheme wherein a frequency-modulated pump laser spin-polarizes Cs atoms in a vapor cell. The polarized atoms undergo precession in a background magnetic field. The precession frequency, called the Larmor frequency, is proportional to the magnitude of the magnetic field. The atomic procession signal, also known as the Larmor signal, is detected by a probe beam. A sensitivity of 1 pT/√Hz is routinely achieved in commercially available sensors of volume less than 20 cc.

Our research reveals that the sensitivity of the magnetometer is mainly limited by the probe VCSEL since it is tuned to be almost exactly resonant with an atomic transition. The resonant probe light interacts strongly with the atoms, not only depolarizing the synchronized atomic spin and hence reducing the Larmor signal, but also introducing more noise into the signal by converting laser frequency noise into the laser intensity noise, which limits the signal-to-noise ratio (SNR) of the measurement. With commercially available narrow-linewidth distributed Bragg reflection (DBR) lasers and off-resonant detection of the Larmor precession, we have demonstrated more than an order of magnitude improvement in sensitivity in the same cell as used in the MFAM magnetometer. We believe that with a better technique to stabilize laser frequency, similar results can also be achieved with VCSEL lasers.

There are two main factors affecting the sensitivity of magnetometers using VCSEL lasers, frequency stabilization and laser linewidth. The simplest and most common laser frequency stabilization method locks the laser to the frequency of an atomic transition using laser current servo that maximizes the absorption of light passing through the atoms. While it is necessary to have the pump laser on resonance in order to achieve the maximum optical pumping, Larmor precession can be detected by off-resonant linearly-polarized probe light through optical rotation. In fact, the SNR of the Larmor signal can be increased by more than an order of magnitude by switching from on-resonant to off-resonant detection. Stabilizing the VCSEL frequency off-resonant from an atomic transition, however, is challenging. We will explore the possibility of off-resonant locking by temperature servo of the VCSEL die. The other factor, laser linewidth, characterizes the fundamental limit on the laser frequency uncertainty. Commercial DBR lasers normally have linewidths ranging from sub-MHz to several MHz. On the other hand, VCSELs have much wider linewidths, typically around 100 MHz. The large noise in the probe laser frequency increases the noise in the detected Larmor signal, hence affecting the magnetometer

sensitivity. In the following section, we propose an intrinsic gradiometer setup, which minimizes the impact of the laser frequency noise on the gradiometer sensitivity.

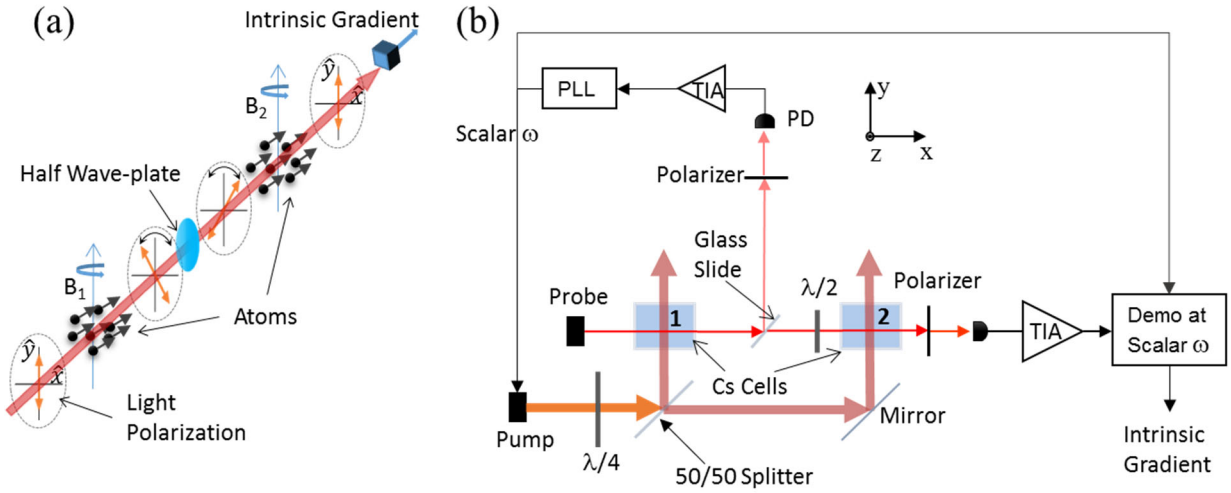

Figure 7 (a) Basic operating principle of an intrinsic gradiometer. (b) Schematics of the intrinsic gradiometer.

The basic principle behind the intrinsic gradiometer is illustrated in Figure 7 (a). A single linearly-polarized off-resonant probe interrogates two atomic ensembles separated by a baseline distance. The atoms at both locations are spin-polarized exactly the same way. After interacting with the first atomic ensemble, the probe goes through a half-wave plate oriented such that the acquired polarization rotation of the probe beam is reversed, as shown in the figure. If the magnetic fields at the two locations are exactly the same, the second ensemble of atoms rotates the probe polarization back to its original position. The optical rotation effect is cancelled. However, if there is a magnetic field gradient, the difference in Larmor frequencies will result in non-cancellation in the rotation of the probe polarization. Therefore, the probe polarization signal is a direct measurement of the magnetic field gradient.

Now we present more detailed analysis of the proposed gradiometer. Assuming that the atomic spin is driven by an oscillating signal $\Omega\cos(\omega t)$, we can write the atomic spin along the x-direction in terms of in-phase (absorptive) and quadrature (dispersive) components with respect to the driving signal, $\Omega\cos(\omega t)$. The spin is then given [5] by $P_{in}\cos(\omega t) + P_{out}\sin(\omega t)$, where

$$P_{x-in} = \frac{R_2^2}{R_2^2+(\omega-\omega_0)^2} P_{x0} \,,$$

$$P_{x-out} = \frac{(\omega-\omega_0)R_2}{R_2^2+(\omega-\omega_0)^2} P_{x0} \qquad (2)$$

Here, R_2 is the transverse spin relaxation rate and ω_0 is the Larmor frequency.

Since the probe polarization rotation, θ, is directly proportional to P_x, θ will have exactly the same dependence on ω as P_x,

$$\theta_{in} = \frac{R_2^2}{R_2^2+(\omega-\omega_0)^2}\theta_0,$$

$$\theta_{out} = \frac{(\omega-\omega_0)R_2}{R_2^2+(\omega-\omega_0)^2}\theta_0 \qquad (3)$$

Some probe light, after passing through the first atomic ensemble, will be split for the scalar magnetometer operation: the driving frequency, ω, will be adjusted so that $\theta_{out} = 0$. According to Equation (3), this guarantees that ω is on average equal to the Larmor frequency ω_0 at the first location and has additive measurement noise such that the instantaneous $\omega \neq \omega_0$. In the gradiometer mode, the second atomic ensemble is also driven by the same frequency, ω. If the difference between the two Larmor frequencies is much smaller than R_2, the overall quadrature polarization rotation is given by

$$(-\theta_{out} + \theta'_{out})|_{\omega\approx\omega_0} = -(\omega - \omega_0)C + (\omega - \omega'_0)C' \qquad (4)$$

where $C=\theta_0/R_2$ and $C'=\theta_0'/R_2'$, are the resonant dispersive slopes at the first and second locations, respectively. As seen, if we match the dispersive slopes, $C=C'$, Equation (4) becomes

$$(-\theta_{out} + \theta'_{out})|_{\omega\approx\omega_0} = (\omega_0 - \omega'_0)C \qquad (5)$$

Based on Equation (5), it is easy to see that the overall quadrature component is proportional to the magnetic field gradient, $(\omega_0-\omega_0')/\gamma$, where γ is the gyromagnetic ratio of atoms. In addition, the noise in the scalar output does not affect the sensitivity of the gradiometer as long as $C=C'$. Frequency noise in the probe affects the optical rotation signal, θ. However, in the intrinsic gradiometer operation, a single probe interrogates both atomic ensembles. The ensembles are only separated by several centimeters, which is much shorter than the laser coherent length. Therefore two atomic ensembles experience the same frequency fluctuation. The resulting optical rotation noise due to the probe frequency fluctuation is cancelled out.

The intrinsic gradiometer can be realized schematically shown in Figure 7 (b). A circularly polarized pump beam is equally split into two beams, exciting Cs atoms at two vapor cells. A linearly polarized off-resonant probe beam interrogates two atomic ensembles at the same time. About 10% light is split from the main probe beam by a piece of glass slide and is detected by a photodiode after an analyzing linear polarizer. The photo current is then amplified and sent to a phase-lock-loop (PLL) circuit. The output of the PLL drives the pump laser through current modulation and is the scalar measurement of the magnetic field at the first cell. After the second cell, the main probe beam is analyzed by a linear polarizer and detected by a photodiode, whose current is amplified and sent to a demodulator with its reference frequency determined by the PLL output. The quadrature component of the demodulated probe signal is converted to the intrinsic gradiometer reading with a constant determined by the slople of the quadrature component at the magnetic resonance.

Results and Discussion

1. Fast Localization of Magnetic Anomalies through Gradient-based Inversion

a. Inversion Method

The magnetic field of a dipole is given by $\boldsymbol{B}_{dipole} = \frac{\mu_0}{4\pi}\left[\frac{3\hat{r}(\boldsymbol{m}\cdot\hat{r})-\boldsymbol{m}}{r^3}\right]$, where μ_0 is the vacuum permeability, $\boldsymbol{m}$ is the vector dipole moment, $\hat{r}$ is the unit vector in the direction of $\boldsymbol{r}$ which is the relative location of the point of interest with respect to the magnetic dipole. With a known background magnetic field $\boldsymbol{B}_0$, the magnetic field of the dipole can be calculated at any location $\boldsymbol{r}$. Based on this, we first establish a full dipole field model, which outputs $\boldsymbol{B}(\boldsymbol{m}, \boldsymbol{B}_0, \boldsymbol{r})$ with input parameters $(\boldsymbol{m}, \boldsymbol{B}_0, \boldsymbol{r})$. With the function $\boldsymbol{B}(\boldsymbol{m}, \boldsymbol{B}_0, \boldsymbol{r})$, it is straightforward to calculate magnetic gradients. The relative location $\boldsymbol{r}$ can be expressed as $\boldsymbol{r} = \boldsymbol{r}_i - \boldsymbol{r}_d$, where $\boldsymbol{r}_i$ is the observing point location and $\boldsymbol{r}_d$ is the dipole location. Now the total gradients at four observing points, shown in Figure 5, can be expressed as $\Delta B_i(\boldsymbol{m}, \boldsymbol{r}_d, \boldsymbol{B}_0, \boldsymbol{r}_i)$, i = 1, 2, 3, 4. To improve the localization accuracy, we also include four vertical gradients in the simulation, $\Delta B_{zi}(\boldsymbol{m}, \boldsymbol{r}_d, \boldsymbol{B}_0, \boldsymbol{r}_i)$, i = 1, 2, 3, 4. All simulation codes are written in Matlab.

The gradient-based localization method can now be simplified as how to find $(\boldsymbol{m}, \boldsymbol{r}_d)$ with a given set of data, $(\Delta B_i, \Delta B_{zi}, \boldsymbol{B}_0, \boldsymbol{r}_i)$. There are no analytical expressions for $(\boldsymbol{m}, \boldsymbol{r}_d)$ in terms of $(\Delta B_i, \Delta B_{zi}, \boldsymbol{B}_0, \boldsymbol{r}_i)$. Therefore, we construct the following function:

$$F(\boldsymbol{m}, \boldsymbol{r_d}) = \sum_{i=1}^{4}\left[\frac{\Delta B_i(\boldsymbol{m}, \boldsymbol{r_d}, \boldsymbol{B_0}, \boldsymbol{r_i})}{\Delta B_i^0} - 1\right]^2 + \sum_{i=1}^{4}\left[\frac{\Delta B_{zi}(\boldsymbol{m}, \boldsymbol{r_d}, \boldsymbol{B_0}, \boldsymbol{r_i})}{\Delta B_{zi}^0} - 1\right]^2 \qquad (6)$$

Here ΔB_i^0 and ΔB_{zi}^0 are measured magnetic gradients at the four points of interest. The best set of dipole parameters $(\boldsymbol{m}, \boldsymbol{r}_d)$ should minimize the function $F(\boldsymbol{m}, \boldsymbol{r}_d)$. To avoid the function being dominated by measured gradients with close to zero values, weight parameters are added to Equation (6):

$$G(\boldsymbol{m}, \boldsymbol{r_d}) = \sum_{i=1}^{4}\left|\frac{\Delta B_i^0}{\max(\Delta B_i^0)}\right|\left[\frac{\Delta B_i(\boldsymbol{m}, \boldsymbol{r_d}, \boldsymbol{B_0}, \boldsymbol{r_i})}{\Delta B_i^0} - 1\right]^2 + \sum_{i=1}^{4}\left|\frac{\Delta B_{zi}^0}{\max(\Delta B_i^0)}\right|\left[\frac{\Delta B_{zi}(\boldsymbol{m}, \boldsymbol{r_d}, \boldsymbol{B_0}, \boldsymbol{r_i})}{\Delta B_{zi}^0} - 1\right]^2 \qquad (7)$$

With a given set of parameters $(\Delta B_i^0, \Delta B_{zi}^0, \boldsymbol{B}_0, \boldsymbol{r}_i)$, we find the minimum value of $G(\boldsymbol{m}, \boldsymbol{r}_d)$ with the built-in Matlab function, *fminsearch*. The corresponding solution $(\boldsymbol{m}, \boldsymbol{r}_d)$ provides us with information about the magnetic dipole, including its location, $\boldsymbol{r}_d$.

b. Inversion Results

The "measured" gradients $(\Delta B_i^0, \Delta B_{zi}^0)$ are generated by the same theoretical model described in the Materials and Methods section. A noise source is also created by multiplying a random number between -1 and 1 with a fixed value and added to each gradient in $(\Delta B_i^0, \Delta B_{zi}^0)$ to represent the measurement error caused by sensor output noise. The fixed value is the peak-to-peak noise amplitude. In practice, the sensor noise is likely to follow the Poisson distribution or the Gaussian distribution, where most noises are around 0. In this work we may not be able to run enough trials to include peak noises, which have the most negative effects on the inversion accuracy. Therefore we simply treat the noise as uniform random numbers to exaggerate the noise effect. We apply the inversion method to the same data sets in Table 2 with the initial dipole magnitude and location

given by Equation (1) and the initial dipole orientation defined by the background magnetic field direction. The peak-to-peak sensor noise is first set at 4 pT. The inversion simulation is then run 10 times for each set of gradient data to account for the random noise. The resulting averaged dipole locations and standard deviations are shown in Table 3 third row. Compared with the results shown in Table 2 (without added noise), the inversion method generates much more accurate dipole locations. We also repeat the inversion simulation for different noise levels. For 40 pT and 100 pT peak-to-peak noises, the results are shown in Table 3 fourth row and fifth row, respectively. As expected, the higher the noise level, the less the accuracy of the inversion method. It can even completely fail as shown in the last two gradient data sets, where the gradient values are only about 200 pT, comparable to the noise level. The resulting dipole orientations are not shown here since the spheroid orientations given in Table 3 are not the actual dipole orientations, which depend on the relative direction between the background magnetic field and the spheroid axis.

Table 3 Localization results from the inversion method for different magnetic dipoles and peak-to-peak noises. The dipole gradients are generated by a spheroid with its orientation and location given in the first two rows.

Orientation (θ, φ)	0°,0°	30°,0°	60°,0°	90°,0°	120°,0°	0°,0°	30°,60°	60°,90°
Set Location (x, y, z)	1 m, 1 m, -1 m	1 m, 1 m, -1 m	1 m, 1 m, -1 m	1 m, 1 m, -1 m	1 m, 1 m, -1 m	1 m, 2 m, -1 m	2 m, 1 m, -0.5 m	2 m, 1 m, -0.5 m
Inversion Results $4pT_{p-p}$ noise	1 ±0.009 m, 1 ±0.007 m, -1 ±0.008 m	1 ±0.001 m, 1 ±0.005 m, -1 ±0.007 m	1 ±0.007 m, 1 ±0.007 m, -1 ±0.01 m	1 ±0.001 m, 1.01±0.006 m, -1 ±0.02 m	0.99±0.01 m, 1 ±0.01 m, -1 ±0.02 m	0.98±0.04 m, 2 ±0.03 m, -1.04 ±0.06 m	1.99 ±0.04 m, 1.01 ±0.02 m, -0.51 ±0.04 m	1.97 ±0.08 m, 1.04 ±0.08 m, -0.49 ±0.08 m
Inversion Results $40pT_{p-p}$ noise	0.99 ±0.09 m, 1.01 ±0.06 m, -0.97 ±0.1 m	1 ±0.04 m, 1.05 ±0.08 m, -0.92 ±0.1 m	0.98 ±0.04 m, 0.98 ±0.07 m, -1.02 ±0.07 m	0.99 ±0.06 m, 1.01 ±0.06 m, -0.97 ±0.1 m	1.1 ±0.2 m, 1.08 ±0.2 m, -0.74 ±0.4 m	1.01 ±0.7 m, 1.78 ±0.7 m, -1.57 ±1 m	1.88 ±0.6 m, 1.11 ±0.4 m, -0.45 ±0.4 m	0.88 ±0.8 m, 0.18 ±0.9 m, -1.76 ±1.6 m
Inversion Results $100pT_{p-p}$ noise	0.95 ±0.2 m, 0.91 ±0.1 m, -1.02 ±0.1 m	0.98 ±0.2 m, 1.1 ±0.3 m, -0.9 ±0.2 m	0.96 ±0.2 m, 0.95 ±0.2 m, -1.07 ±0.3 m	1.08 ±0.2 m, 1.1 ±0.3 m, -0.74 ±0.3 m	0.97 ±0.4 m, 0.88 ±0.3 m, -0.78 ±0.5 m	0.48 ±0.9 m, 1.62 ±1.4 m, -1.09 ±1.5 m	0.38 ±0.6 m, 0.27 ±1.8 m, -1.92 ±1.3 m	-0.48 ±5.4 m, -0.6 ±2.7 m, 0.16 ±3.1 m

Based on the results shown in Table 3, 4 pT peak-to-peak noise level is required for gradient measurements. If we assume a 10 ms measurement time, 4 pT peak-to-peak noise is equivalent to a r.m.s. noise density of about 100 fT/√Hz, which is an order of magnitude less than the noise density achieved in our MFAM sensors. Much better sensors need to be developed for the gradient based inversion method.

2. A Portable Prototype Intrinsic Magnetic Gradiometer

a. Off-resonant Frequency Stabilization of VCSEL lasers

As discussed in the Materials and Methods section, one of the main challenges of the project is to realize the off-resonant frequency stabilization of VCSEL lasers. We use 895 nm VCSEL packages from Vixar. The VCSEL is mounted on a Thermo-Electric-Cooler (TEC) temperature controller with a temperature-sensing thermistor inside a TO-5 package. The TEC and the thermistor are then connected to a TED 200C temperature controller box from Thorlabs. We set up a benchtop

magnetometer system to study the efficacy of the off-resonant frequency stabilization using the above temperature controlling system.

The benchtop magnetometer is schematically shown in Figure 8. Two VCSEL packages are used as the "Pump" and "Probe" light sources with laser temperatures stabilized by TED 200C boxes. The two light beams cross inside a 5 mm x 5 mm x 5 mm Cs vapor cell placed at the center of a 4-layer magnetic shield can. The same Cs vapor cells are used in the portable gradiometer. The pump light becomes circularly polarized after a quarter-wave plate while the probe light is linearly polarized when interacting with Cs atoms. The transmitted probe beam is analyzed by a linear polarizer and detected by a photodiode, whose photocurrent goes through a transimpedance amplifier with a gain of 100 kΩ (not shown). The amplified signal is then sent to a Phase-Lock-Loop (PLL) electronic system from Zurich Instrument. The PLL outputs the Larmor frequency, which can be converted to the magnetic field reading by the gyromagnetic ratio, 3.498572 Hz/nT, of Cs atoms. The PLL output also controls the current modulation frequency of the pump VCSEL.

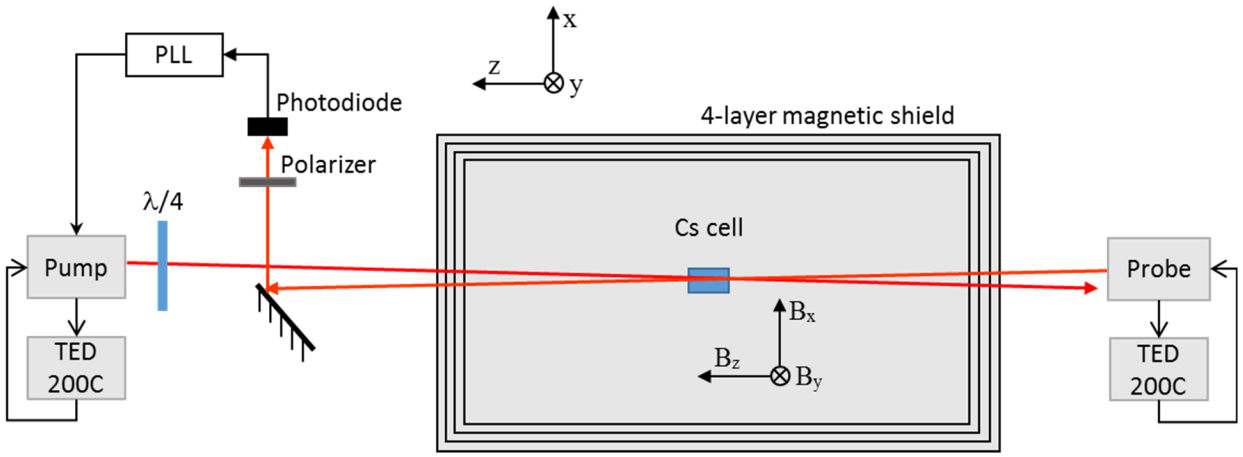

Figure 8 Schematics of a benchtop magnetometer.

Since the frequency stability of the VCSEL laser directly affects the magnetometer output noise, we characterize the performance of the frequency stabilization method by measuring the magnetometer noise. The pump VCSEL laser is resonant on the |F=3> → |F'=4> transition of Cs D1 line and its current is modulated by the PLL output. The pump beam has a total power of about 300 μW. The probe VCSEL laser is about 10 GHz blue detuned with respect to the |F=4> → |F'=3> transition of Cs D1 line with about 150 μW in power. Both lasers have Gaussian spatial profile with FWHM of about 1.8 mm. The Cs vapor cell is heated to about 68ºC. After optimizing the VCSEL temperature stabilization circuit through PID control of the TED 200C electronics, we are able to achieve better than 150 fT/√Hz magnetometer output noise density, shown in Figure 9. The increase in the noise density below 30 Hz is mainly due to air current along the beam paths, causing fluctuation of the air refractive index, which affects the polarization of the beams. The sharp spikes

in Figure 9 are due to the couplings of the 60 Hz power line radiation and its harmonics into the electronics.

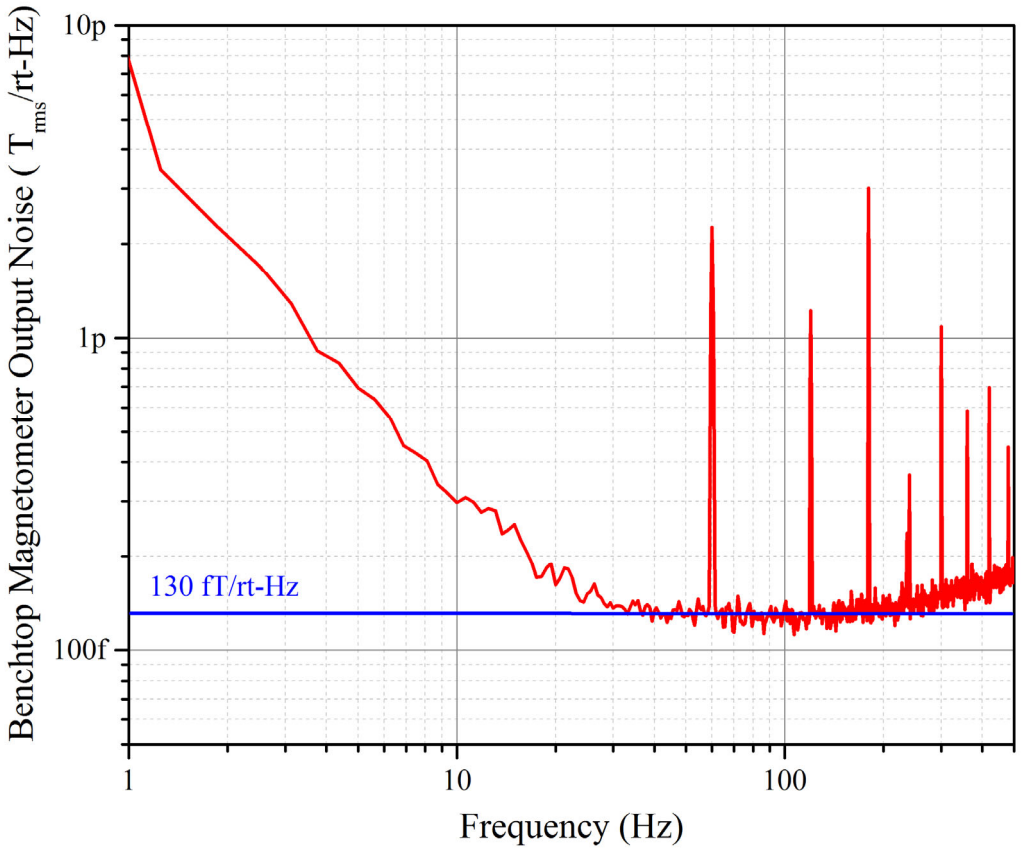

Figure 9 Output noise density of a benchtop magnetometer with off-resonant linearly polarized probe light.

The demonstrated noise density shown in Figure 9 may be limited by the magnetic shield can, not by the fundamental magnetometer performance. To investigate this possibility, we operate the magnetometer in an open-loop setup, rather than the closed-loop PLL. In the open-loop setup, the amplified probe signal is sent to a lock-in amplifier with the reference frequency set by the pump current modulation frequency. Magnetic resonance of the magnetometer can be measured by recording the lock-in outputs while scanning the pump modulation frequency around the Larmor frequency. Both the in-phase and the quadrature components of the lock-in amplifier are shown in Figure 10 (a). We also measure the amplitude spectral density of the probe photodiode signal after the transimpedance amplifier. As shown in Figure 10 (b), 300 nV/√Hz noise density is achieved. Combining the slope, 2.1 mV/Hz, of the quadrature component at the resonant frequency (Larmor frequency) with the 300 nV/√Hz noise density in the probe photodiode and the 3.498572 Hz/nT gyromagnetic ratio, we can calculate the fundamental magnetometer noise density as 300 nV/√Hz / (2.1 mV/Hz) / (3.498572 Hz/nT) = 40.8 fT/√Hz. This analysis indicates even better noise performance of the magnetometer, which further validates the off-resonant frequency stabilization method implemented in the benchtop magnetometer setup.

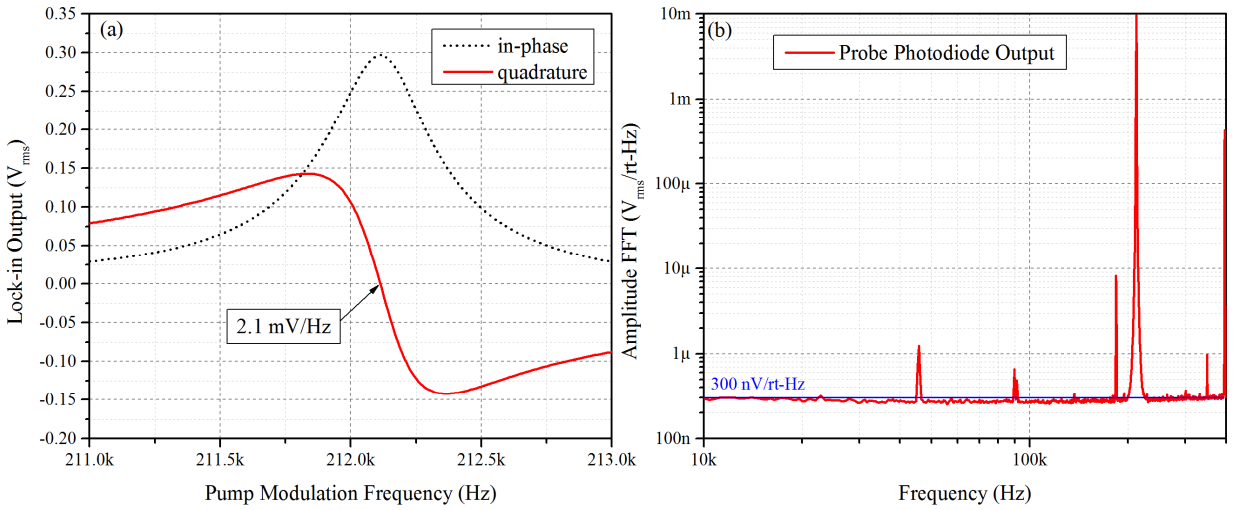

Figure 10 (a) Probe lock-in signal (r.m.s. amplitude) as a function of pump modulation frequency *f*. The black dot (red solid) curve represents the in-phase (quadrature) component. (b) Amplitude spectral density of the probe photodiode signal after the transimpedance amplifier.

b. Intrinsic Magnetic Gradiometer Design

After validating the off-resonant frequency stabilization of VCSEL lasers, we design a layout of optical components for a portable intrinsic gradiometer, shown in Figure 11. Two Cs cells have the inner dimension of 5mm x 5mm x 5mm (not including the tip) and are separated by a center-to-center distance of 5 cm. Out of VCSEL packages, both pump and probe beams are collimated to have a Gaussian FWHM of about 1.8 mm and sent through a linear polarizer for polarization cleanup. After the polarizer, a quarter-wave plate is used to convert the pump light to circularly polarized light. A half-wave plate is also present in the pump path to maximize the pump power after the quarter-wave plate. The circularly polarized pump beam is then split by a 50/50 beam splitter. Half of the beam goes upwards through Cs cell 1 while the other half is reflected by a prism mirror and goes through Cs cell 2. The linearly polarized probe beam travels through cell 1 and is then reflected by two prism mirrors before enters cell 2. Between the prism mirrors, about 10% of probe light is split by a glass slide. Both the main probe beam and the split probe beam are analyzed by a linear polarizer before focused onto a photodiode. The pump beam through cell 2 is also focused onto a photodiode. The photodiode currents are amplified through transimpedance amplifiers with a gain of 100 kΩ for the pump beam and the split probe beam and 200 kΩ for the main probe beam. VCSEL packages, photodiodes and amplifier circuits are mounted on a customized 10cm x 7cm PCB board. The cells are separated by a distance of about 12 cm from the VCSEL packages and 15 cm from the PCB board. In principal, these large separations are not necessary. However, the commercially available VCSEL package is quite magnetic and many IC components on the PCB board are also magnetic. With much smaller separations, the magnetic noise produced by the VCSEL package and the PCB board will affect the performance of the gradiometer. Customized non-magnetic electronics are beyond the scope of this project.

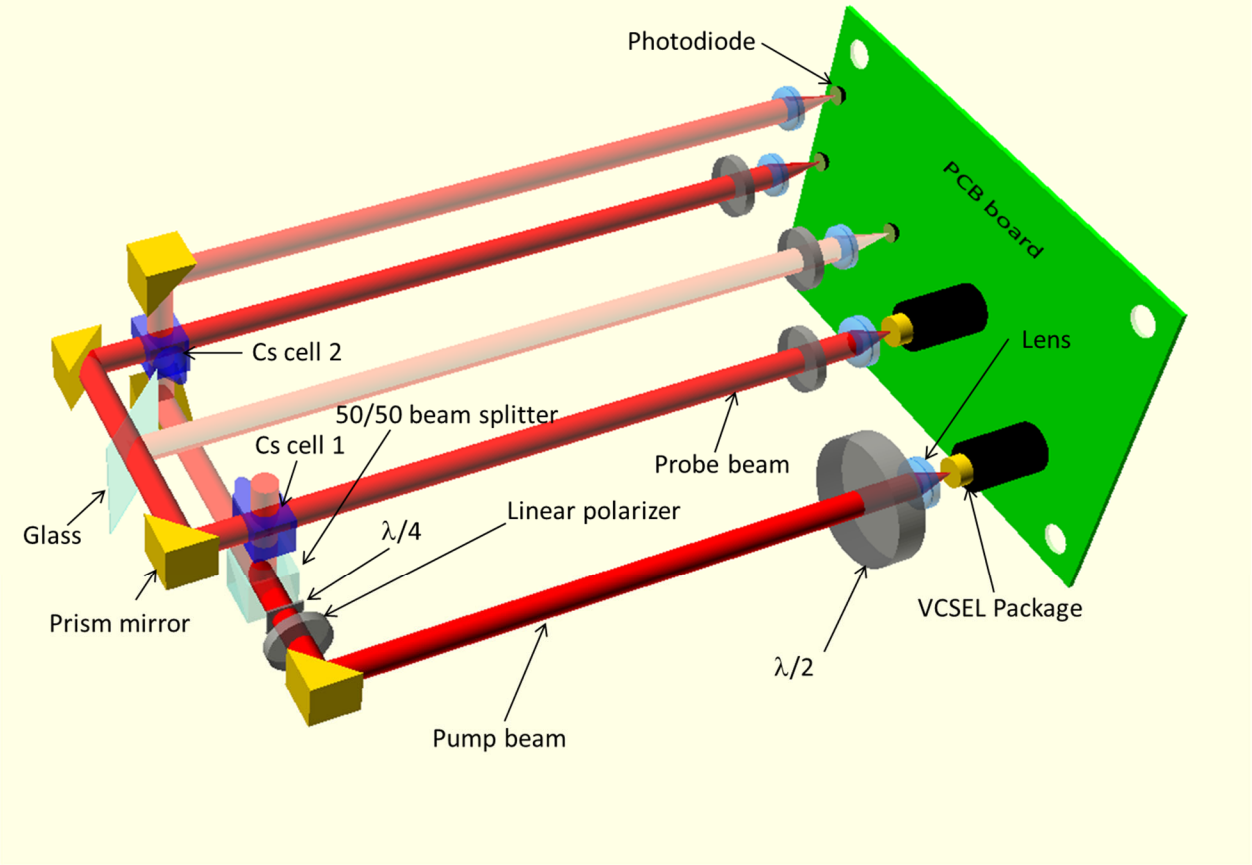

Figure 11 Layout of optical components for a portable intrinsic gradiometer.

According to the optical component layout shown in Figure 11, we explore a couple of concepts regarding how to assemble the portable intrinsic gradiometer. The stacked design, shown in Figure 12, is chosen based on its simplicity. However, the design lacks flexibility of adjustments of optical components, especially the prism mirrors, which turns out to cause quite some trouble when the gradiometer is assembled. The 3D model of the design is first created using SolidWorks software. The real holders are then made using non-magnetic plastics through 3D printing technology. Despite lots of trouble aligning laser beams, we are able to assemble the gradiometer successfully. A partially assembled gradiometer is shown in Figure 13. To avoid optical misalignment inside the gradiometer during its movement, the optical components are glued to the holders.

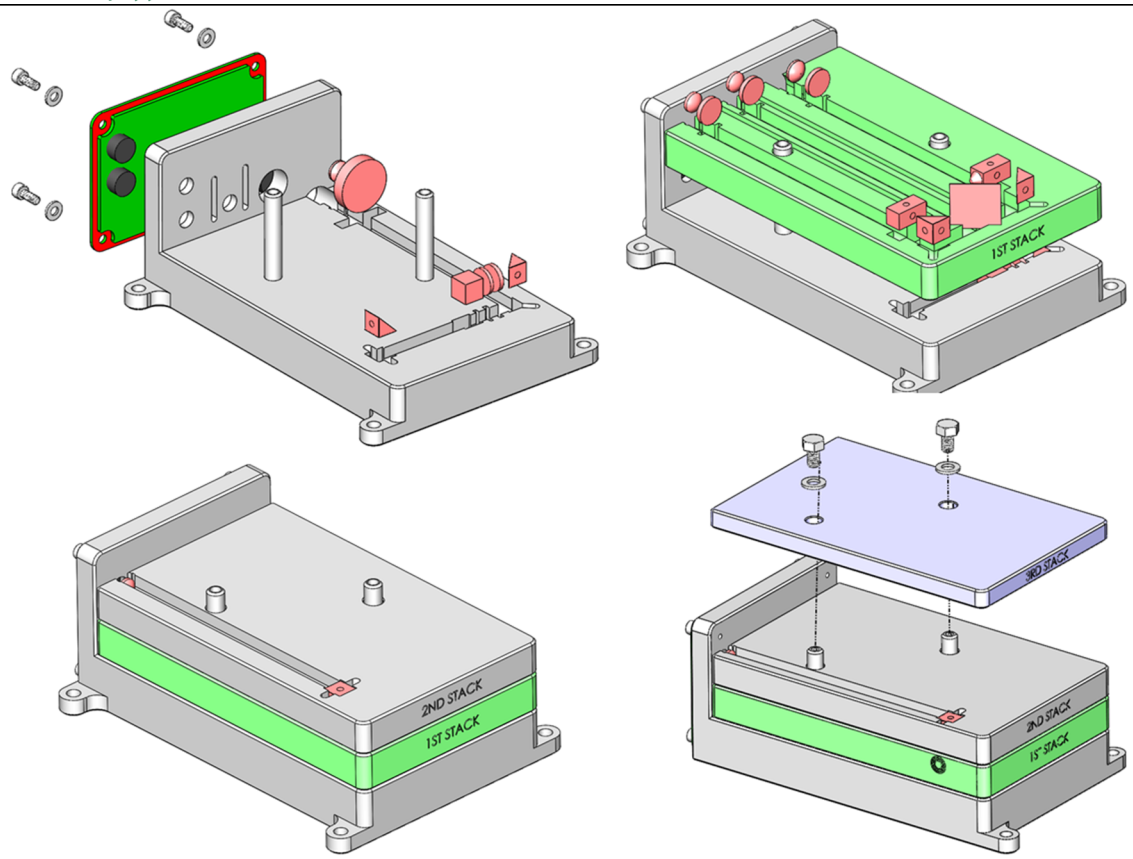

Figure 12 3D model of optical component holders for the intrinsic gradiometer.

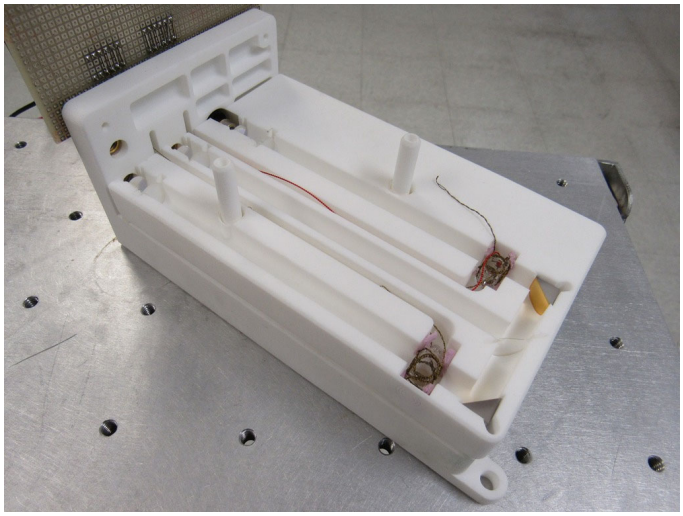

Figure 13 Partially assembled intrinsic gradiometer.

c. Intrinsic Magnetic Gradiometer Performance

The assembled gradiometer is first tested inside a magnetic shield can made of 3-layers of Mu-metal, shown in Figure 14. The magnetic field inside the shield can is generated using a solenoid controlled by a home-made ultra-low-noise current source. The field strength is set to be about 63,600 nT. Ideally, the sensing locations, where the two Cs cells are, should be along the axis of the solenoid. However, as shown in Figure 14, the Cs cells are clearly off-axis. Our original plan

was to use a much bigger shield can. But initial testing results indicated undermined shielding ability of the bigger shield can. The gradiometer noise performance was limited by the environmental noise inside the bigger shield can.

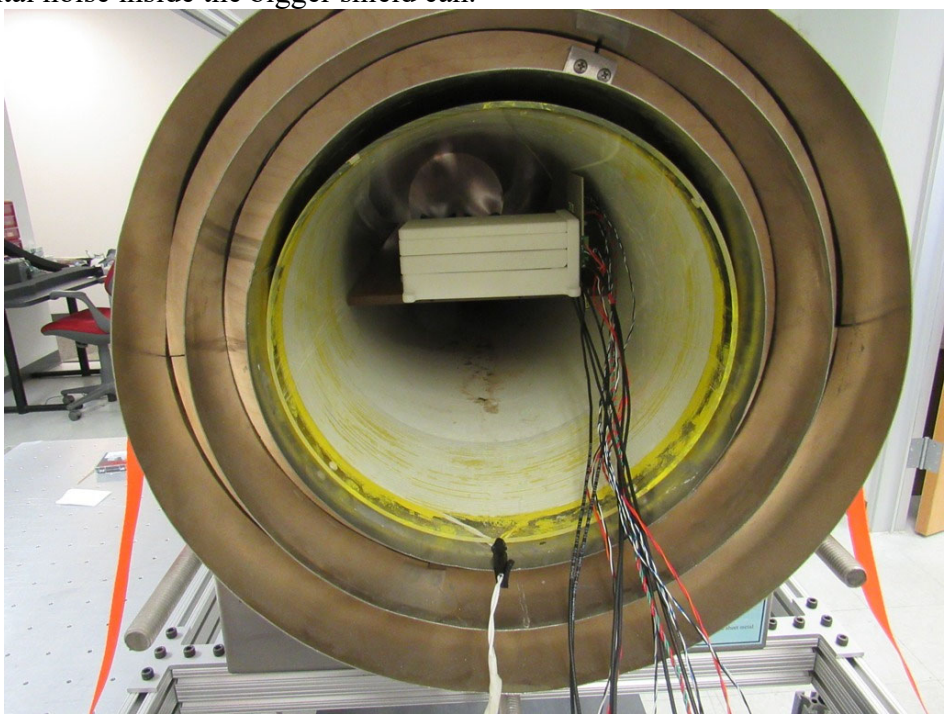

Figure 14 Portable intrinsic gradiometer inside the shield can.

We first test the scalar magnetometer operation with the split probe beam. As shown in Figure 7 (b), the scalar magnetometer measures the magnetic field at the cell 1 location. Before operating the scalar magnetometer in closed-loop mode, we measure the magnetic resonance signal and the split probe photodiode noise spectral density, shown in Figure 15. The results are obtained similarly as in Figure 10. Combining the 0.29 mV/Hz slope of the quadrature components at the magnetic resonance and the 300 nV/√Hz noise density in photodiode signal, we can estimate the output noise density of the scalar magnetometer in closed-loop mode to be about 300 fT/√Hz, which is confirmed in Figure 17.

To optimize the operating parameters of the intrinsic gradiometer, we measure the magnetic resonances at individual cells. The procedure is similar to the one previously described for the result shown in Figure 10. However, since the main probe beam goes through both cells, the resonance signal at one cell is recorded while the pump beam for the other cell is blocked. For the optimal gradiometer performance, the resonant slopes of the two quadrature components need to be matched, as discussed in the Material and Methods section. The optimized magnetic resonance signals are shown in Figure 16 (a). As seen, the resonance signal at cell 2 has exactly the opposite phase as that at cell 1. The two quadrature components have the same slope amplitude of 2.1mV/Hz but with opposite signs. If the two quadrature signals are added as in the case when both cells are excited by modulated pump beams, the combined signal is directly proportional to the magnetic field gradient, defined as the field difference between the two cells. Due to the imperfect matching parameters, such as the Cs cell buffer gas pressure and the overlapping between the pump and probe beams, and the fact that a portion of probe beam going through the first cell is split, the two resonance signals have different amplitudes while the slopes at resonances are matched. We also

measure the main probe photodiode noise spectral density to be about 550 nV/√Hz, as shown in Figure 16 (b). The estimated gradiometer output noise density is then 550 nV/√Hz / (2.1 mV/Hz) / (3.498972 Hz/nT) = 75 fT/√Hz.

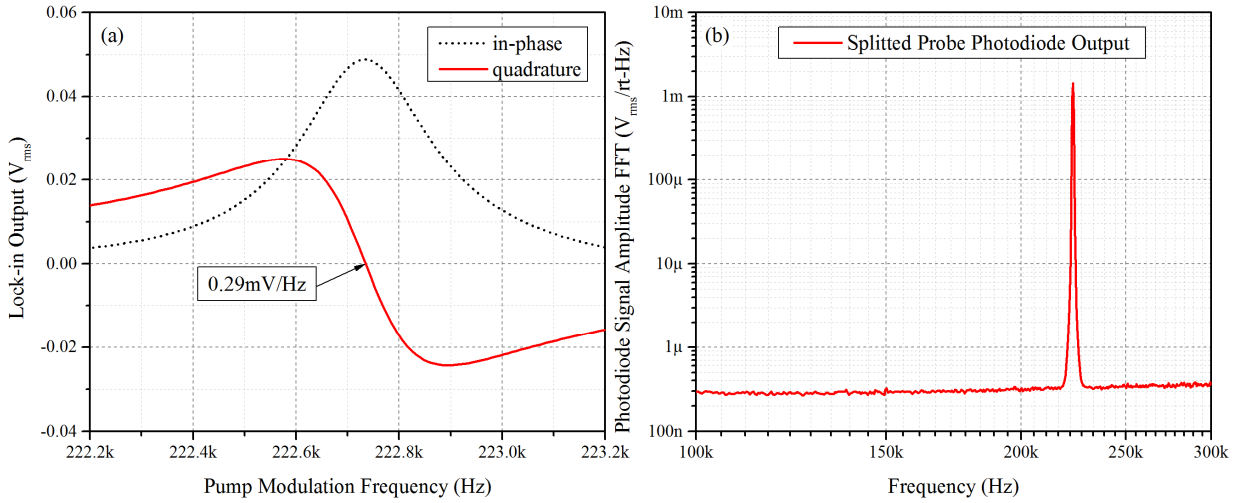

Figure 15 (a) Split probe lock-in signal (rms amplitude) as a function of pump modulation frequency *f*. The black dot (red solid) curve represents the in-phase (quadrature) component. (b) Amplitude spectral density of the split probe photodiode signal after the transimpedance amplifier.

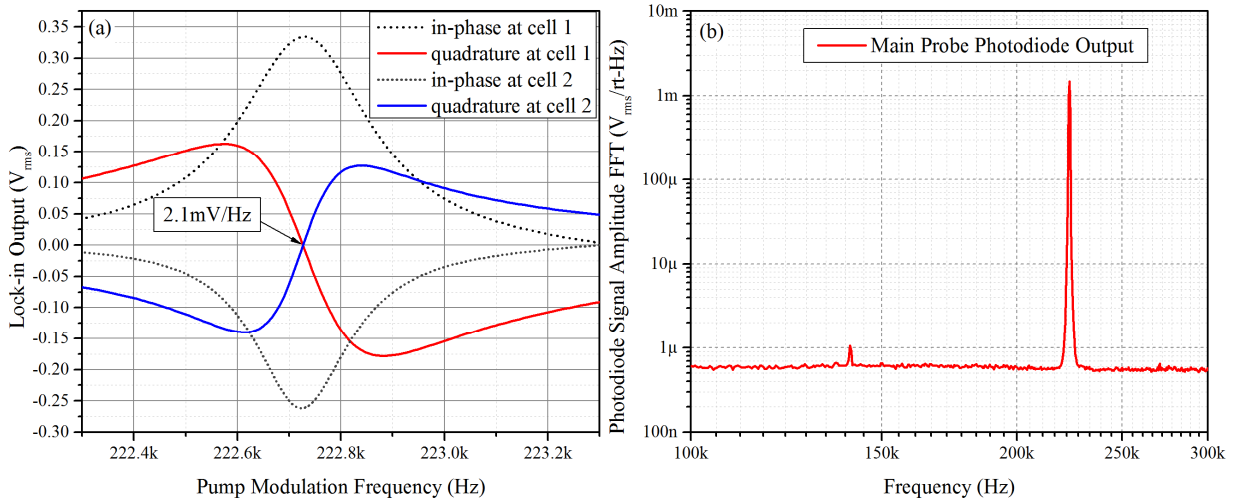

Figure 16 (a) Main probe lock-in signal (rms amplitude) as a function of pump modulation frequency *f*. The black dot (red solid and blue solid) curves represent the in-phase (quadrature) components at two cells. (b) Amplitude spectral density of the main probe photodiode signal after the transimpedance amplifier.

We now operate the scalar magnetometer in the closed-loop mode using Zurich Instrument PLL. The output of the PLL is the scalar reading and also the reference frequency of the demodulator used to extract the quadrature component. The quadrature signal is then converted directly to the gradient output by the coefficient 0.1361 nT/mV calculated based on the slope 2.1mV/Hz and the gyromagnetic ratio, 3.498972 Hz/nT. The output noise densities of both the scalar magnetometer and the intrinsic gradiometer are shown in Figure 17. As seen, the gradiometer noise density reaches below 90 fT/√Hz. This is higher than the estimated gradiometer noise density of 75 fT/√Hz, possibly due to the environmental gradient noise (a little over 40 fT/√Hz environmental gradient noise can explain the observed difference). Nevertheless, this still clearly demonstrates a

major advantage of the intrinsic gradiometer: its noise is less than that of a gradiometer consisting of two scalar magnetometers with the same components. Two scalar magnetometers with a noise density of 75 fT/√Hz can only generate a gradient measurement with no better than √2*75 fT/√Hz = 106 fT/√Hz noise level. The sharp spikes here are due to the couplings of the 60 Hz power line radiation and its harmonics into the electronics.

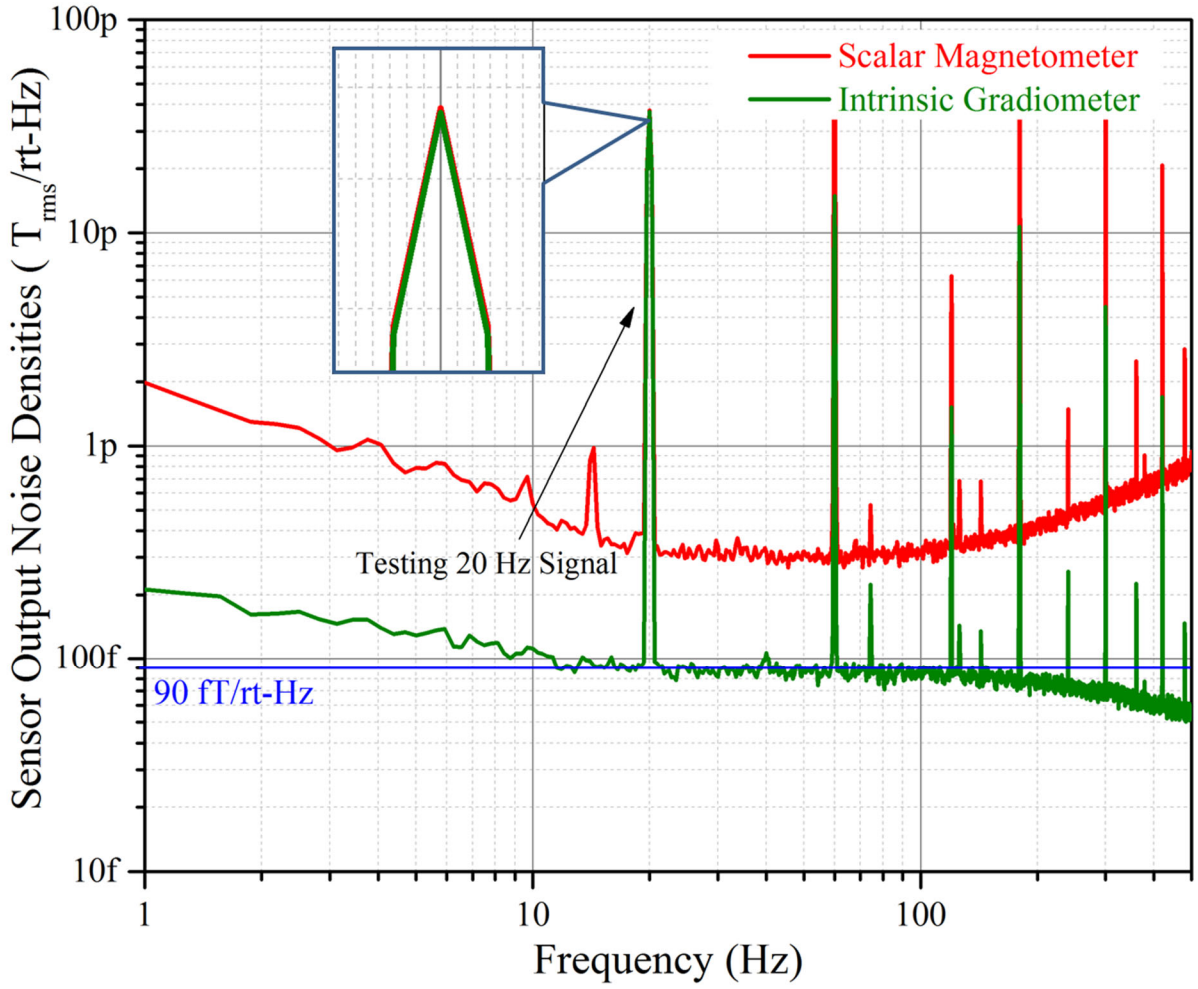

Figure 17 Output noise densities of both the scalar magnetometer (red curve) and the intrinsic gradiometer (green curve). A 20 Hz testing signal is also generated by a 3 mm diameter coil right next to cell 1. The signal should have the same amplitude in both outputs.

The accuracy of the gradiometer conversion coefficient is further verified by a 20 Hz testing signal. The signal is generated by a 3 mm diameter coil attached to cell 1. Since the distance between cell 2 and the coil is more than a factor of 10 larger than the coil diameter and that between cell 1 center and the coil and the fact that magnetic dipole signal decays as $1/r^3$, the signal should be a factor of more than 1000 smaller at cell 2 as that at cell 1. Therefore the amplitude of the 20 Hz testing signal measured by the scalar magnetometer (measuring fields at cell 1) should be almost the same as that measured by the intrinsic gradiometer if the conversion coefficient is accurate. This is confirmed as shown in Figure 17.

Another interesting analysis regarding the gradiometer noise performance is how much it is limited by the photon shot noise, which often sets the practical limit of atomic magnetometers. For a light

power of p, the photon shot noise has a flat amplitude spectral density of $\sqrt{(2hvp)}$, where hv is the single photon energy. The total probe power after the analyzing linear polarizer is 26 μW. With p = 26 μW, λ = 895 nm, photodiode efficiency of 0.65 A/W and 200 kΩ transimpedance amplifier gain, the noise floor of the amplitude spectral density due to the photon shot noise is about 440 nV/√Hz, which is not much lower than the 550 nV/√Hz noise density demonstrated in Figure 16 (b). This close-to-photon-shot-limit achievement is significant considering the fact that only VCSEL lasers are used in the intrinsic gradiometer. The achievement paves the way towards practical miniaturized gradiometers with ultra-low noises once only realizable inside research labs.

We also measure the bandwidth of both the scalar magnetometer and the intrinsic gradiometer. Signals with the same amplitude but varying frequencies are generated by the same 3 mm diameter coil. The signal amplitudes at different frequencies are measured by both the scalar magnetometer and the intrinsic gradiometer. The normalized amplitude, gain of the sensor, is plotted as a function of frequency, shown in Figure 18. As seen, the scalar magnetometer has a 3-dB bandwidth of about 300 Hz while that of the intrinsic gradiometer is about 150 Hz.

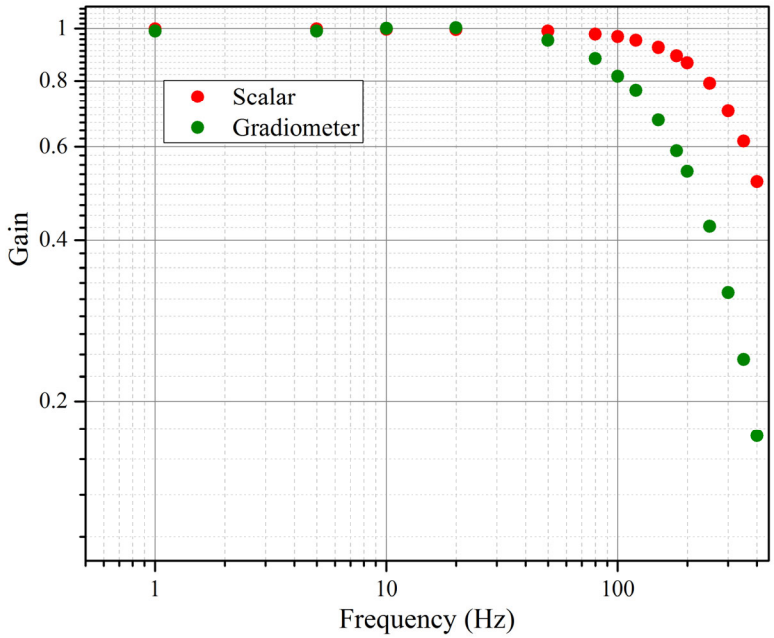

Figure 18 Bandwidth of the scalar magnetometer (red dots) and the intrinsic gradiometer (green dots).

3. Gradiometer Performance in Unshielded Environment

a. Gradiometer Noise in Unshielded Environment

After demonstrating and characterizing the gradiometer performance inside the shield can, we move the sensor outside the magnetically shielded environment. The gradiometer is mounted to a non-magnetic rotatable platform located in an office inside a commercial building. The setup is shown in Figure 19. The platform is rotated such that the Earth's magnetic field is close to the direction along the two cells. Electronics, especially computers, are kept at distances as far away from the gradiometer as possible. The noise performance of the gradiometer in the Earth's magnetic field is shown in Figure 20. Compared with the noise performance inside the shielded environment (Figure 17), gradiometer noise increases by a factor of 2 while the scalar noise is more than 20 times worse for frequencies below 60 Hz. The signal at 60 Hz and its harmonics are almost 3 orders of magnitude larger. This is expected since all electric currents inside the building

contribute to the environmental magnetic noise, which is measured by the scalar magnetometer. However, the gradiometer has a very short baseline (5 cm separation between the two cells). Since most noise sources are much further away compared with the baseline distance, they generate common mode noises at two cell locations. The common mode noises are automatically rejected by the gradiometer. As a result, the gradiometer performance does not suffer as much in the unshielded environment. Note that the result in Figure 20 is achieved inside a building where many magnetic noise sources are present and nearby. We expect better gradiometer noise in field applications since most likely there will be fewer noise sources with greater distances from the sensor.

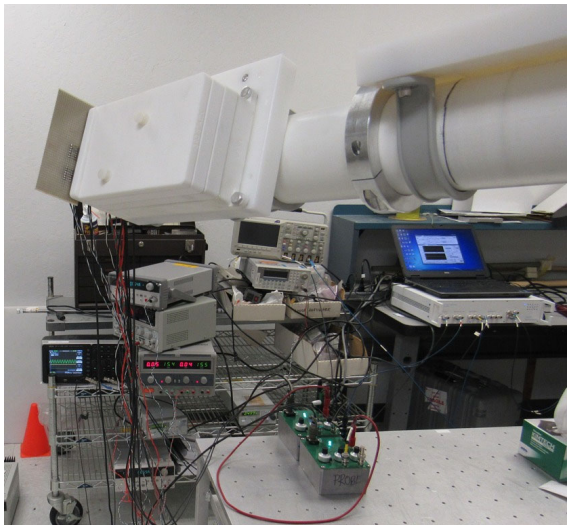

Figure 19 Intrinsic gradiometer in a magnetically unshielded environment.

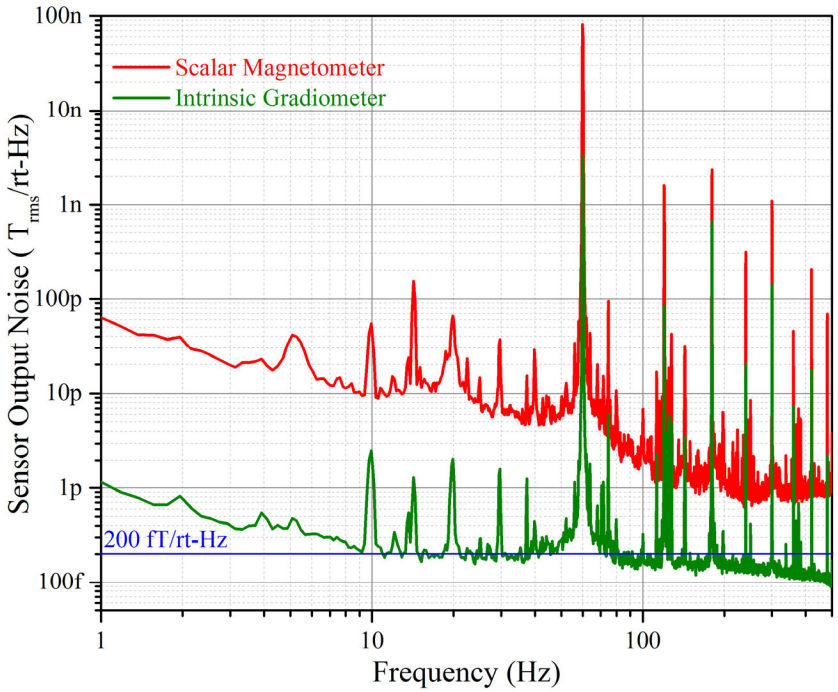

Figure 20 Output noise densities of both the scalar magnetometer (red curve) and the intrinsic gradiometer (green curve) in a magnetically unshielded environment.

b. Magnetocardiography using Intrinsic Gradiometer in Unshielded Environment

To demonstrate the sensitivity of the gradiometer, we attempt Magnetocardiography, which is a measurement of the magnetic fields generated by electrical currents in the heart, using the setup shown in Figure 19. A researcher stands beside the setup for a few seconds while the gradiometer outputs are recorded. The raw data is shown in Figure 21 (a). As expected, the raw gradiometer data is dominated by the 60 Hz noise produced by the AC electrical currents in the building. The 60 Hz noise can be filtered out by a notch filter. Based on the noise density plot shown in Figure 20, a low-pass filter is also needed in order to filter out higher frequency spikes. After passing the raw data through a 60 Hz notch filter and a 70 Hz low-pass filter, we plot the result in Figure 21 (b). As seen, the intrinsic gradiometer is clearly sensitive enough to detect the heart beat signals.

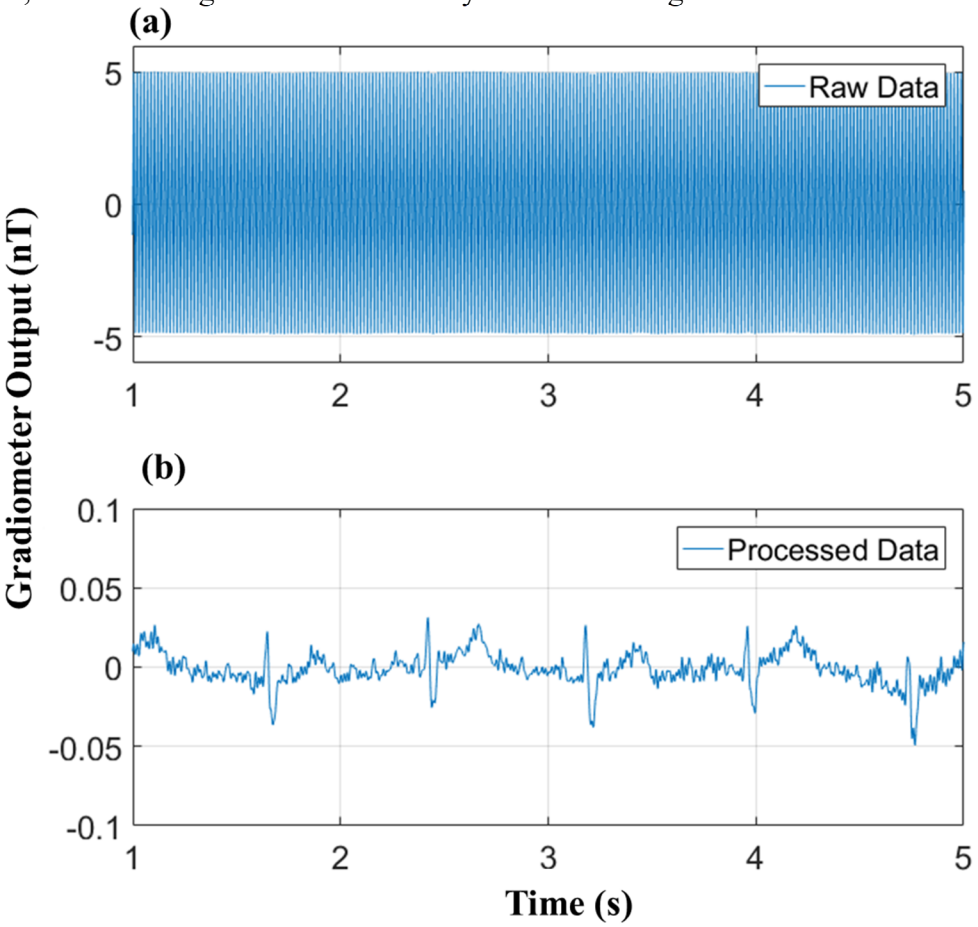

Figure 21 Measurement of the magnetic fields generated by heart beats using the intrinsic gradiometer in the unshielded environment. (a) Raw gradiometer data. (b) Same data after passing through a notch-filter at 60 Hz and a low-pass filter at 70 Hz.

4. Limitations and Challenges

a. Effect of Multiple UXOs on Inversion Method

The gradient based inversion method discussed in the previous section works only for a single magnetic dipole moment in the vicinity of the gradiometers. If there are multiple dipole moments contributing to the gradient signals, the inversion method will become much more complicated. It is very likely that a simple 4-point gradient measurement may not be enough to determine multiple UXO locations. The efficacy of gradient based fast localization of multiple UXOs still needs further investigation.

b. Limits of Intrinsic Gradiometer

The intrinsic gradiometer demonstrated in the previous section has limited linear response range. As discussed in the previous section, the gradiometer output is determined by the slope of the quadrature component shown in Figure 16 (a). As seen, the slope is only linear around the magnetic resonance frequency. The linear range is about ± 15 Hz (±4 nT), which should also be the linear response range of the gradiometer. To investigate the linear response range, we apply a testing signal similar to the one shown in Figure 17. The testing signal has a fixed frequency at 5 Hz with different amplitudes. Both the scalar output (with a constant offset) and the gradiometer output are recorded and displayed in Figure 22. If the signal amplitude is beyond the linear range of the gradiometer, the relative amplitude of the gradiometer, defined as the ratio of the measured gradient amplitude to the scalar amplitude, will be less than one. As seen in Figure 22 (a) and (b), both relative amplitudes are about one when the signal peak-peak amplitude is below 10 nT. When the peak-peak amplitude is slightly above 10 nT, shown in Figure 22 (c), the relative amplitude starts decrease, which becomes obvious in Figure 22 (d) where the signal amplitude goes beyond 40 nT. This investigation proves the inaccuracy of the gradiometer if the gradient is more than ~ 2 nT/cm (10 nT linear range divided by the distance between two cells). The gradient tolerance can be increased if we shorten the cell separation.

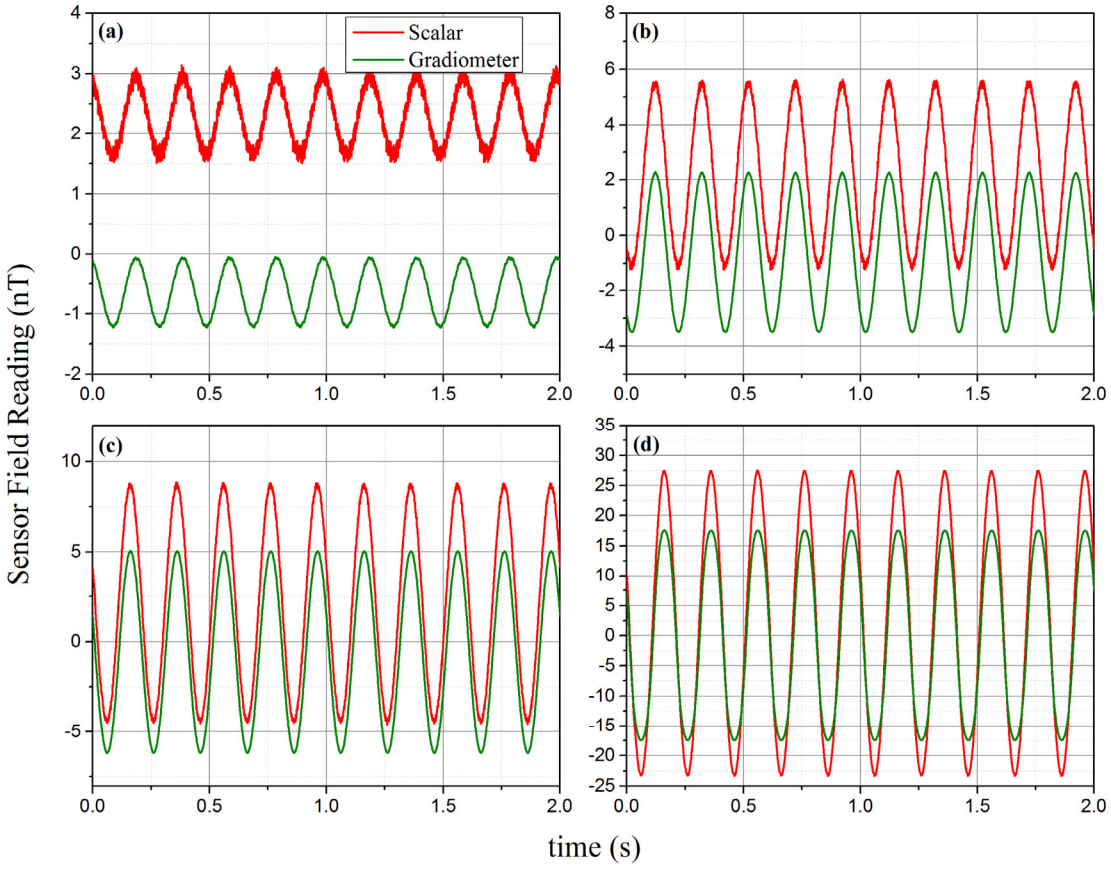

Figure 22 Scalar (red curve) and gradiometer (green curve) measurements of a 5 Hz signal generated by the 3-mm diameter coil right next to cell 1. The signal has different amplitudes in (a), (b), (c) and (d).

c. Heading Error

Due to the dependence of the interaction between atoms and light on the orientation of the magnetic field relative to the light propagating direction, the quadrature slope shown in Figure 16 (a) is

affected by the gradiometer orientation with respect to the background magnetic field. In the current gradiometer setup, the gradient reading is converted directly from the quadrature component with a constant determined by the slope. Therefore there will be heading errors in the gradient measurement. In principal, this issue may be fixed by applying an auto-gain controller to the lock-in signal input. Before the demodulation, all signals will have the same amplitude at the cost of increased noises for smaller amplitude signals. As long as the quality factor of the magnetic resonance remains the same, the slope becomes independent of the relative sensor orientation to the magnetic field.

Conclusions and Implications for Future Research

A magnetic-gradient-based inversion algorithm for real-time localization of a magnetic dipole moment is developed. Simulation work indicates that real-time localization with high accuracy (~ 1cm) is possible using short-baseline gradiometry with high sensitivity. For a 100 Hz sample rate, 100 fT/√Hz gradient noise density at 5 cm baseline is required by the inversion algorithm.

A portable intrinsic gradiometer is shown to meet the sensitivity and baseline requirements of the gradient-based inversion algorithm. A gradient sensitivity of better than 100 fT/√Hz at 5 cm baseline is achieved. The successfully demonstrated portable gradiometer is composed of miniaturized vapor cells and VCSEL lasers, two components essential for achieving compact sensor packages. The success of the project eliminates the fundamental scientific risk of obtaining ultra-sensitive short-baseline magnetic gradient data in practical applications.

The gradient measurement can be used for real-time UXO localization with high accuracy, greatly reducing the cost of UXO disposal by shortening the time-consuming localization procedure. Current classification methods using time domain electromagnetic (TDEM) require very high accuracy in real-time target localization to position the instrument over the target – this new localization method enhances reacquisition efficiency and accuracy and may be integrated with TDEM instruments to reduce location-based uncertainty in classification results.

More efforts are necessary towards a field demonstration of the gradient-based real-time UXO localization. The next step is to build field-worthy ultra-sensitive gradiometers, including designing a more-compact sensor package and developing an integrated sensor driver. Considering the limits of the intrinsic gradiometer and the sensitivity of the scalar magnetometer shown in Figure 9, a gradiometer consisting of two scalar magnetometers may be a better approach for ultra-sensitive and short-baseline gradient measurements. In addition, more theoretical modeling work is needed to study the impact of multiple UXOs on the localization accuracy. These efforts can lead to magnetic gradient measurement with unprecedented sensitivities and short-baselines and hence may enable many more novel applications of the magnetic gradiometry in UXO detection and classification.

Literature Cited

[1] S. D. Billings, L. R. Pasion and D. W. Oldenburg, "Discrimination and Identification of UXO by Geophysical Inversion of Total-Field Magnetic Data," ERDC/GSL TR-02-16, U.S. Army Corps of Engineers, Washington DC, 2002.

[2] W. Doll, "Demonstration of an Enhanced Vertical Magnetic Gradient System for UXO," ESTCP project MM-0633, 2008.

[3] A. Salem, T. Hamada, J. K. Asahina and K. Ushijima, "Detection of unexploded ordnance (UXO) using marine magnetic gradiometer data," *Exploration Geophysics,* vol. 36, pp. 97-103, 2005.

[4] W. E. Bell and H. L.Bloom, "Optically driven spin precession," *Phys. Rev. Lett.,* vol. 6, p. 280, 1961.

[5] S. J. Seltzer, "Developments in Alkali-Metal Atomic Magnetometry," PH.D. Dissertation, Princeton, 2008.